Scanning Force Microscopy Studies of Purple Membrane Monolayers

A Proposal

Submitted to the Advisory Committee

at

Purdue University

for

Scott Crittenden

In Partial Fulfillment of the

Requirements for the

Preliminary Examination

February 2000

TABLE OF CONTENTS

Page

LIST OF TABLES

LIST OF FIGURES

Figure Page

Figure Page

1. Introduction

The Nanoscale Physics Lab at Purdue University has, for many years, studied electronic properties of single molecular monolayers deposited on metal substrates. The membrane protein, bacteriorhodopsin (bR), a component of the purple bacterial-membrane (Purple Membrane, PM) of the salt-marsh-loving bacteria *Halobacterium salinarium* (HS) has been, and is, the subject of intense study by many groups of researchers in many disciplines, generating, in one form or another, thousands of peer reviewed research papers over the last few decades.

I claim that bR is a natural extension of the Nanoscale Physics Lab's work to biological molecules. Besides being generally considered interesting by outside researchers, bR extends the Lab's domain of study. bR is larger, more complex, and possesses distinctly different qualities than the set of molecules previously and currently studied by the Lab. Furthermore, previous work by other researchers on PM has focused almost exclusively on studies in the bulk, frequently of spectroscopic properties. With the notable exception of H. J. Butt's electrostatic work,[1–4] Scanning Probe Microscopy (SPM) studies of PM have been incidental to the work being reported; techniques have been developed and then applied, merely by way

of demonstration, to PM. This presents the Lab with the opportunity to apply our current skills to a domain both new to us and interesting to others. Additionally, the photoactivity of bR and its small size make it a natural candidate for a nanoscale photodetector, something which would be of interest to the semiconductor industry as it approaches molecular scale component sizes.

I propose to study, with various Scanning Force Microscopy (SFM) techniques at the nanoscale level, the properties of PM patches deposited on various substrates with an eye toward possible device applications, improved investigative techniques, and extending the group's current theoretical models of molecular monolayers. I would like to develop protocols and techniques that can be readily extended to any biological material of interest.

This report presents work performed to date, provides analysis of preliminary results, and proposes future areas of investigation and specific experiments. In outline, Chapter 2 gives an overview of PM, Chapter 3 presents an overview of SFM theory and apparatus to be used, Chapter 4 is an overview of relevant previous PM research and of my preliminary results, and Chapter 5 discusses proposed work.

2. bR, PM, and *Halobacterium Salinarium*

I propose to study the purple cellular membrane of the bacterium *Halobacterium salinarium*. I present below a brief discussion of biological terms and facts relevant to the understanding of what a cellular membrane is and why this particular one was chosen for this study.

2.1 The Things Living Things are Made of

Starting small and working toward the big, I will begin not with quarks and leptons, but with atoms, and stop, a little before water buffalo, with individual cells. Specifically I mention the six kinds of atoms that make up the vast majority of all biological entities: Carbon, Hydrogen, Oxygen, Nitrogen, Sulfur and Potassium. These are arranged in a large number of ways to form organic milcules, a subset of all known molecules.

Organic molecules are further subdivided into various families, one of the most important being amino acids. From these, larger molecules, 'proteins', are formed by stringing multiple amino acids together. Proteins (and other biological molecules) make up cells. See Fig. 2.1.

The multitudinous kinds of cells can be grouped into various categories. For our purposes there are two: prokaryotes and eukaryotes. As shown in Fig. 2.2,

prokaryotes are smaller (by a factor of 10^{-3} in volume) and simpler than eukaryotes (six commonly recognized components *vs.* nine).[5] Eukaryotic cells make up all multicellular organisms and have a bewildering variety of internal structures, none of which are of concern for this study. Prokaryotic cells also have an amazing, but lesser, number of internal structures which vary over the different eukaryotic organisms.

2.2 Bacteria and *Halobacterium salinarium*

The next step up the ladder of complexity is no step at all. The smallest living things (neglecting philosophical debates about virii and prions) are single celled creatures. One type is the bacterium (there are others, amoebae for instance). Bacteria are prokaryotes, and as such are rather simple compared to the eukaryotic cells that make up plants and animals. They possess a cell wall and (one or more) cell membranes.

We are interested in one particular bacterium, *Halobacterium salinarium* (HS) (formerly called *Halobacterium halobium*, references to both may simultaneously appear in the literature),[6] approximately 0.5μm in diameter and 4–10μm long.[7] Living mainly in salt marshes, HS is one member of a small group of bacteria that process sunlight to produce energy without using chlorophyll. All other living things, including some bacteria, which run on sunlight use some form of chlorophyll-based photosynthesis similar to that used by plants. HS also possesses some characteristics of eukaryotic cells and there is some evidence that it is quite

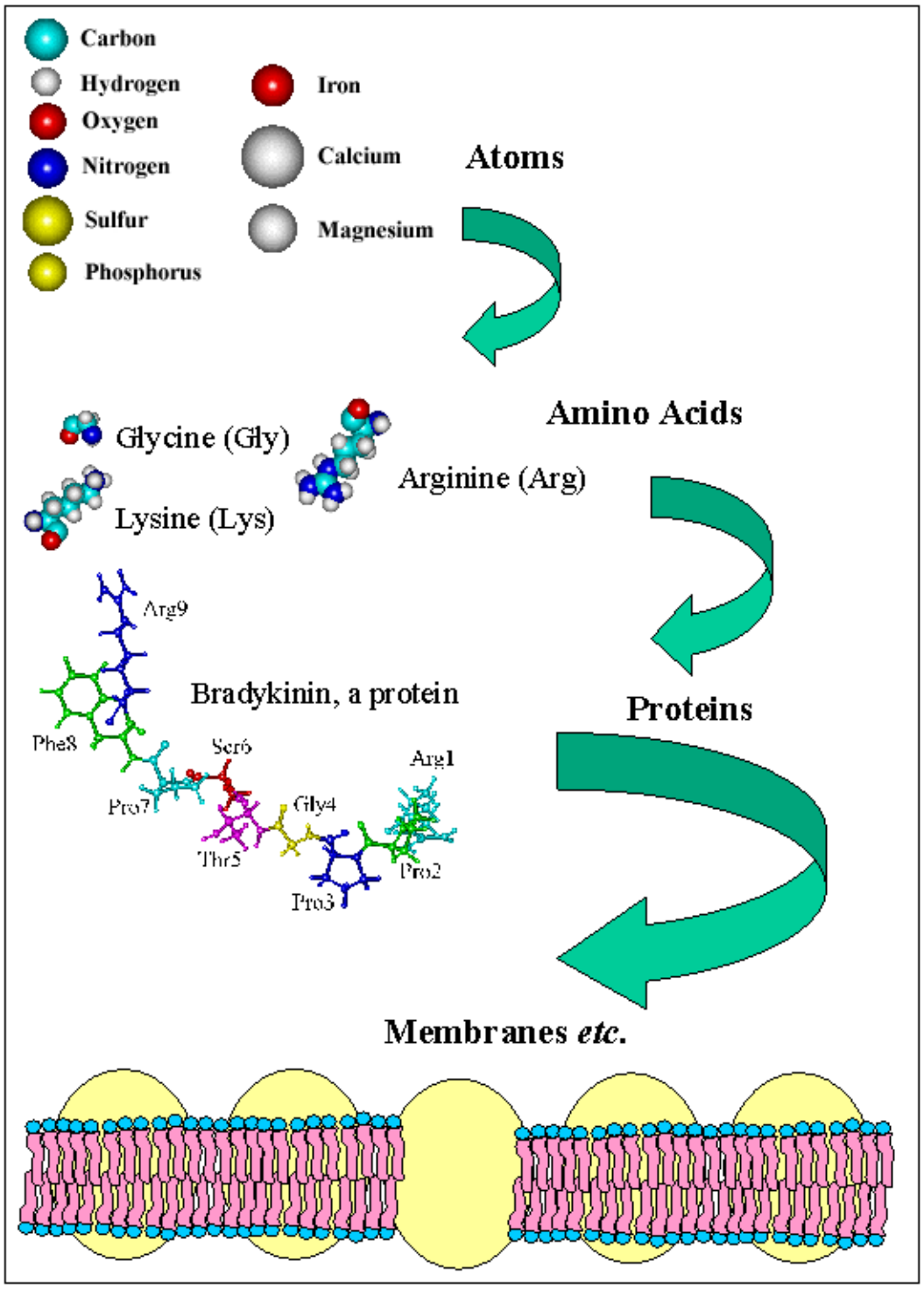

Figure 2.1

Hierarchy of structures from atoms to cell components. Other atomic species, molecules, and structures, exist in the average cell. Shown here are only the most common of each.

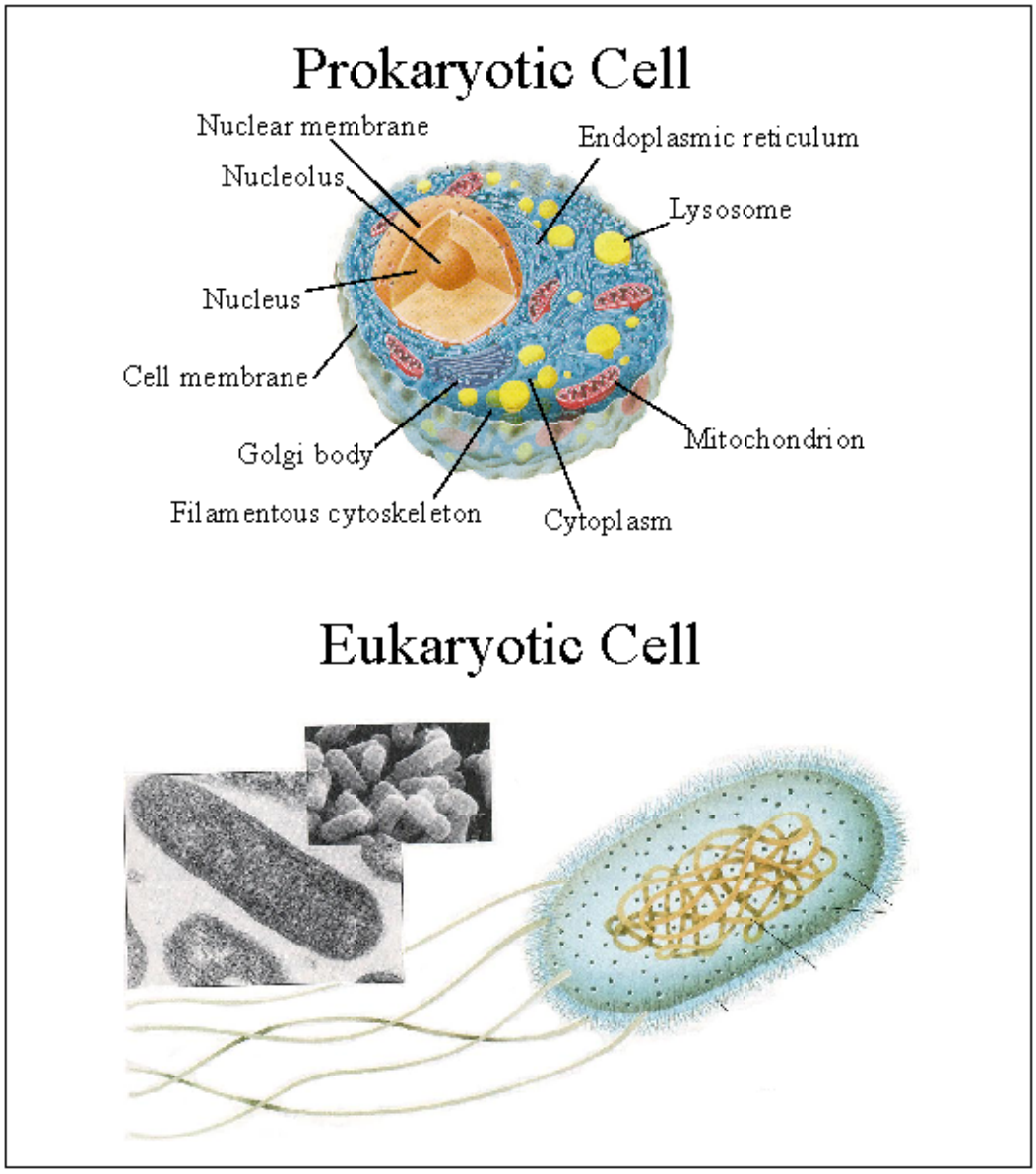

Figure 2.2

The two cell types: Prokaryotic and Eukaryotic. Not shown are plant cells which are significantly different than either. Most single celled organisms are made of prokayotic cells and most multicellular organisms of eukaryotic ones. The increased complexity and size of multicellular organisms is mirrored in increased complexity and size of eukaryotic cells. *H. salinarium* is a prokaryote possessing some features usually seen only in eukaryotes and plants. Adapted from Biochemistry, Second Edition, by Garrett and Grisham.

old on the biological time scale.[7]

2.3 And Back Down a Ways

HS's ability to run on sunlight is made possible by a single protein and its associated lipids. This protein, bacteriorhodopsin (bR), is produced by the bacterium when it senses that it has entered a highly ionic environment, i.e. the salt marsh becomes extra salty. Few things can survive in salt marshes, even fewer in very salty ones, so very salty means very little food exists. In reaction, HS produces bR and some associated lipids. These two molecules enter the bacterium's cellular membrane and form a hexagonally close packed lattice. A large fraction of the cell's membrane can be taken up by the bR-lipid complex.[7] These sections of the membrane are purple in color, hence its name. The rest of the membrane, the normal part, is red and unsurprisingly referred to as Red Membrane. The bacterium uses the PM to generate its standard energy-carrying molecule, ATP, and thus survive in the unpleasant environment.

Fortunately, it is easy to extract PM from HS cultures (killing the HS in the process).[7] The PM occurs in the bacterium in roundish patches, usually of a few hundred nanometers diameter. PM consists of one single protein, bR, surrounded and held in a hexagonal lattice (lattice constant 6.3 nm)[8] by a lipid bilayer. Various sources quote different percentages of protein and lipid making up the membrane but 80% and 20%, respectively, are reasonable ballpark figures.[7]

The lipids serve only to hold the bR molecules in position, and to some extent,

in form. In the jargon of the field, bR is a dichroic chromophore retinal and serves the bacterium as a transmembrane proton pump (Fig 2.3). In other words, bR is light sensitive, i.e. it undergoes a chemical and electronic change under illumination, the probability of absorption of a photon is polarization dependent, and it contains, as its primary active component, a derivative of the molecule called Retinol (otherwise known as a Vitamin A aldehyde). The top and bottom of the bR protein protrude from the lipid bilayer and, when in the proper environment, the net result of absorbing a photon is the net translation of a free H^+ ion from one side of the membrane to the other. Furthermore, this is accompanied by the formation of a momentary dipole field along the membrane-perpendicular axis of the bR.

This dipole is of significant interest in this study. Why? A glance at Fig. 2.3 shows that bR is only about thirty-two cubic nanometers in volume. The dipole is photoactivated (with a quantum efficiency $\sim 60\%$[9]) and produces, at the surface of the protein a few hundred mV potential. Thus bR is a highly efficient molecular-scale electro-optical converter, of great interest to the semiconductor industry as device sizes are projected to approach molecular dimensions within the next few decades. PM is robust (it has been shown to operate in pH environments of 3 to 10 and temperatures of up to 410 K[10,11]). It is easy to produce; the PM self-assembles and the bR contained in it are all atomically identical. All these properties make PM a good candidate for study with SFM techniques.

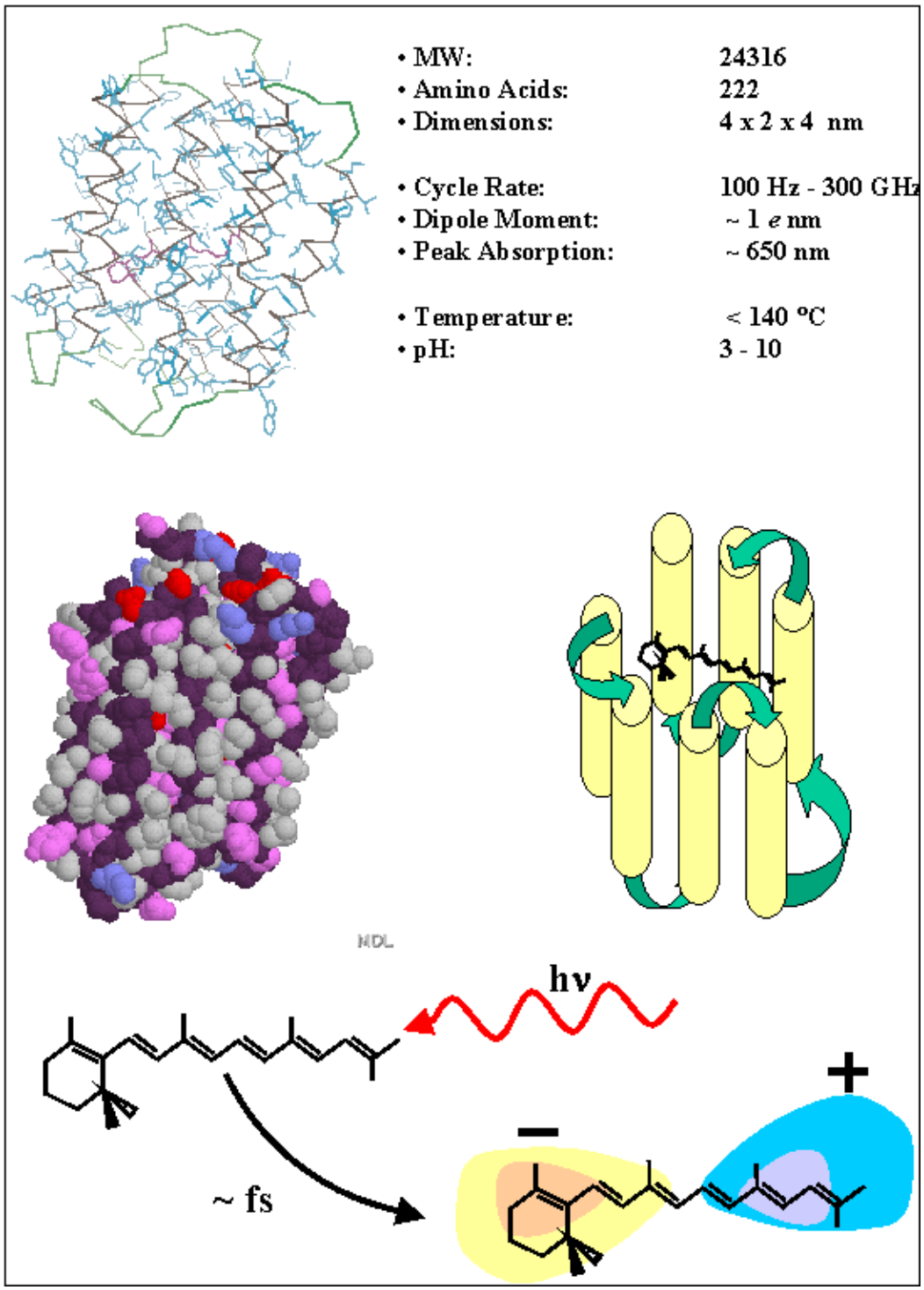

Figure 2.3

Bacteriorhodopsin. bR is composed of seven α-helices (strings of amino acids which take roughly linear helical form) surrounding the 'active' retinol which, after absorbing a photon, developes a momentary dipole moment. Structure information from the Protein Data Bank (structure #1C3W).

3. SFM Theory and Apparatus

The primary measurement apparatus used in this study will be the Scanning Force Microscope (SFM), historically called the Atomic Force Microscope. The SFM is one of three common types of Scanning Probe Microscopes (SPM), of which the others are the Scanning Tunneling Microscope (STM) and the Scanning Near-field Optical Microscope (SNOM). The STM detects currents, the SNOM, photons, and the SFM, electronic forces. Since I don't anticipate using STM and the laboratory doesn't have SNOM capability, you will hear no more of them.

The various types of SPM differ in important ways, but each one measures tip-sample interactions. There is always a Tip, always a Sample over which the tip is moved, and always a method to move this sample in a controlled manner with an effective resolution of 0.1 nm or less.

Almost all SFM techniques (of which there are about ten[12]) detect, in one way or another, the flexure of a small cantilever. These cantilevers, both commercially available and custom made, are usually, but not always,[13] a few hundreds of microns long, a few tens wide, and between two and less than one thick (Fig. 3.1). Both single beam and triangular cantilevers are common as illustrated in Fig. 3.1. Almost all cantilevers have sharp tips at the very end and it is (usually) the forces

on this tip which are responsible for the flexure.

Various techniques are used to detect motion of the cantilever. The most common is optical detection via a multi-segment photodiode of a mW laser focused on the back of the cantilever, henceforth termed the "beam-bounce" method. Another optical method used in one of the SFMs in the laboratory is fiber-optic based Michelson-Morley interferometry. I will describe only the first method as it is most common and the details of the interferometric method are not relevant, as the resulting measurements are the same. Finally, some cantilevers are constructed from piezoresistive materials. Here a deflection of the cantilever is accompanied by a change in its resistance, which is measured and recorded. We have no SFM that uses this detection method.

All SPMs move the sample relative to the tip with the same type of device: a piezoelectric, usually a multielectrode cylinder (commonly called a piezotube). Application of voltage differences between different electrodes causes expansion or contraction of segments of the tube, allowing for approximately linear motion in all three spatial dimensions. Sensitivities of these piezotubes range from a few to a few hundred nanometers per Volt.

Figure 3.2 shows the canonical beam-bounce SFM. Note that there are other important components shown in the figure, namely a feedback loop, and that the photodiode has four segments. This photodiode schematic mirrors the physical one in form; their are four segments arranged in a square.

The laser emits a beam, which is focused on the back of the cantilever and

a)

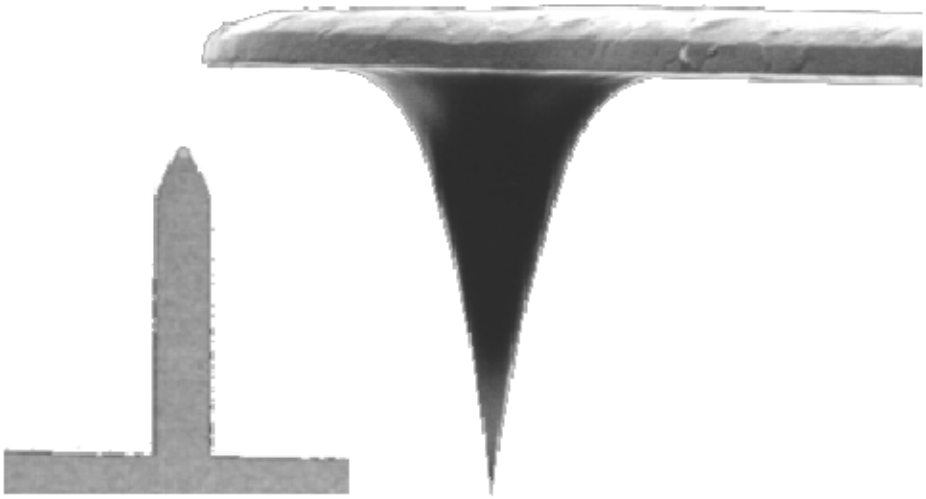

b)

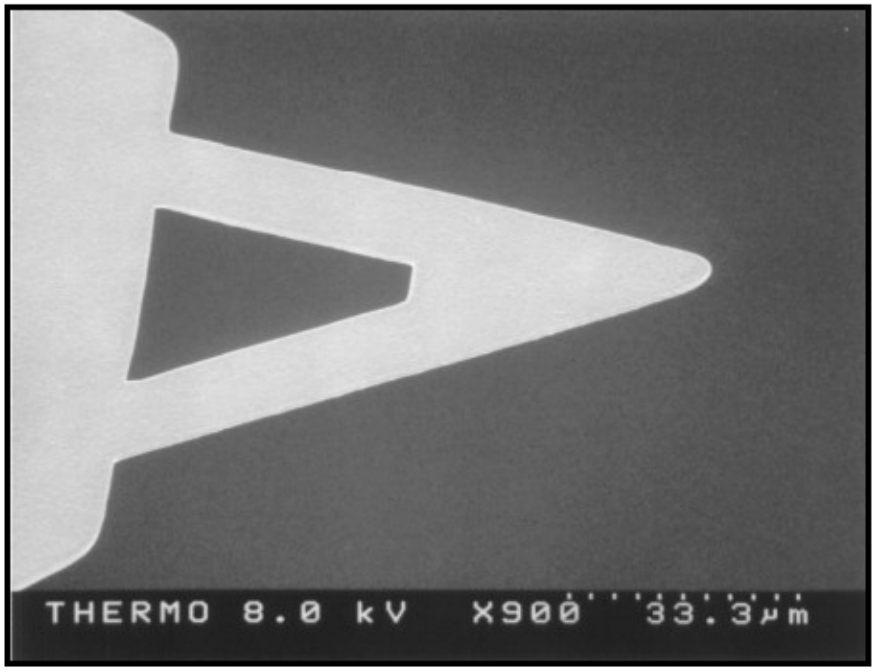

Figure 3.1

SFM cantilevers are usually made of Si (with a thin layer outer Silicon Oxide) or SiN. Both single beam, a), and 'triangular', b), are common. Resonance frequencies range from a few tens to a few hundreds of kHz. Effective spring constants between 0.01N/m to $\sim$ 100N/m are commonly available. Beams are 100–200μm long, $\sim$ 1μm thick, and a few tens of μm wide. Tips are 4–15μm high with end radii most commonly $\sim$ 20nm, although a few are available with radii $\simeq$ 2nm. These don't survive contact with the surface and so must be used in one of the noncontact SFM modes. Images from ThermoMicroscopes, Inc.

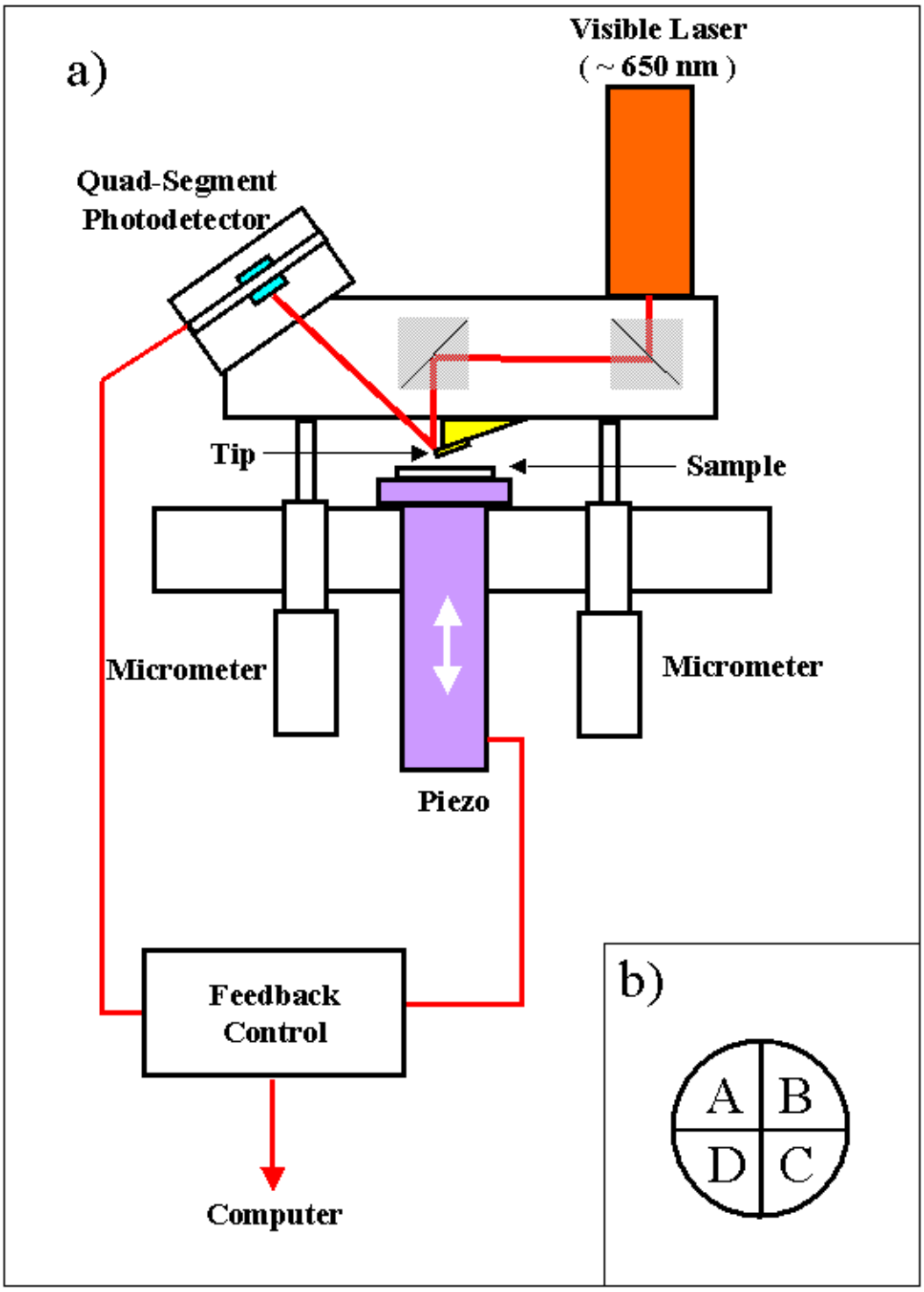

Figure 3.2

Fundamental components of a beam-bounce Contact SFM. a) There is a cantilever which is bent by a sample mounted on an XYZ piezo and off of which a laser reflects into a photodiode. The piezo scans in X and Y while control and monitoring electronics use a feedback loop to maintain constant bending of the cantilever while recording the Z voltage applied to the piezo. b) The photo-diode has four segments arranged in a square to allow both normal and lateral beam motion to be sensed.

reflected from it onto the surface of the photodiode. As the cantilever moves over the sample, it flexes up and down and twists left and right (due to induced torques from friction between the tip and the sample). These cantilever movements result in movements of the laser beam over the photodiode. Measuring the current from the four segments one can infer how the cantilever is bent. Specifically (Fig. 3.2b), (A + B) - (C + D) gives the vertical flex of the cantilever and (B + C) - (D + A) gives its twist.

More explicit descriptions require a choice of one of the many different types of SFM — briefly, which signal is used to control the feedback loop (or loops) is different for different SFM types. I expect to use six kinds of SFM: Contact SFM, Lateral Force Microscopy (LFM), Adhesive SFM, Conductive SFM (CSFM), Noncontact SFM (NC), and Electrostatic Force Microscopy (EFM). I discuss each in that order. See Fig. 3.3

3.1 Contact SFM

Here the tip of the cantilever is brought into mechanical contact with the surface of the sample and kept there throughout the data taking session. The signals from the photodiode when the cantilever is not in contact are taken as reference. A set-point, corresponding to a certain deflection of the cantilever from this equilibrium position, is chosen; typically around one nanometer. As the tip is scanned over the sample (or the sample is scanned under the tip - both methods are common), the feedback loop adjusts the voltage on the piezotube (and hence its vertical

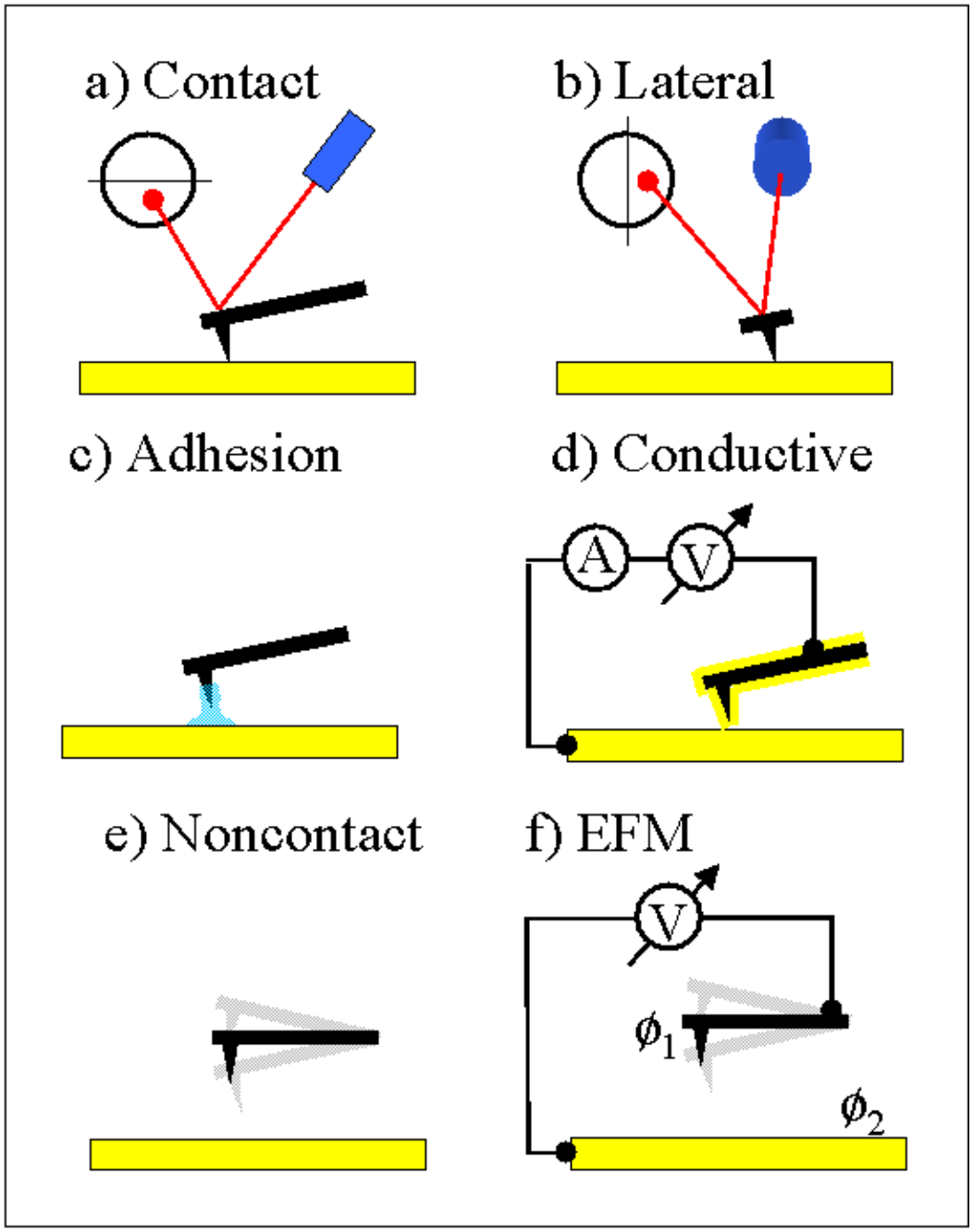

Figure 3.3

The six kinds of SFM I propose to utilize during this study. a) Contact, b) LFM, c) Adhesive SFM, d) CSFM, e) Noncontact, and f) EFM.

extension) so as to attempt to keep the cantilever deflection constantly at the set-point.

This voltage data is used to construct, one pixel at a time, an image of the topography of the surface. Additional signals, specifically the flex and twist of the cantilever, can be simultaneously recorded. These produce, "error signal" and "lateral force" images of the surface.

Were the feedback control perfect, there would be no variation in flexure of the cantilever, hence the data measuring the flex of the cantilever is called the error signal. That this is non-zero can be used to say something about the surface and the quality of the data collected. The error signal can also be used to correct the topography data.

3.2 Contact Pressures and Areas

Typical SFMs can sense normal displacements of the cantilever of 0.1nm or less. Commercially available cantilevers have force constants between 0.01 and 100nN/m. Tips are well modeled as hemispheres with radii of 10–50nm. Piezotubes can produce vertical extensions up to a few microns. From these numbers one can conclude that forces between 1pN and 100μN can be applied.

Commercial SiN tips have tip radii of $\sim$ 20nm and elasticities given in Table 3.2. From this data we can estimate the approximate area of contact between the cantilever tip and the substrate. The various models of elastic contact areas (Hertzian, JKR, etc.) produce essentially the same results for contact forces of

$\sim$ 1nN, which are common in practice. Using the simplest Hertzian theory[14] and taking the tip to be a sphere of radius R and the sample a gold plane we find, where E, G, R, and F are the Young's Modulus, Rigidity Modulus, radius of the tip, and applied force, respectively, using

$$r = \left(\frac{3RF}{4E^*}\right)^{1/3} \tag{3.1}$$

$$E^* = \left(\frac{1-\nu_{tip}^2}{E_{tip}} + \frac{1-\nu_{sample}^2}{E_{sample}}\right)^{-1} \tag{3.2}$$

$$\nu_i = \frac{1}{2}\frac{E_i}{G_i} - 1 \tag{3.3}$$

and the relevant values in Table 3.1 (where r, the E_i, and ν_i are the radius of the contact area, elastic moduli, and Poisson ratios of the tip and sample) we find a contact radius of $\sim$ 0.6nm for a 1 nN applied force. The pressure is then $\sim$ 930MPa.

Table 3.1

Elastic Properties of Gold and Silicon

	Au (GPa)	Si (GPa)	
E	78	170	Young's Modulus
G	27	50	Rigidity Modulus
B	220	—	Bulk Modulus
ν	0.44	0.70	Poisson's Ratio

From these results we can conclude that true atomic resolution in air or in vacuum is unlikely using Contact SFM, which is indeed the case. In practice it is difficult to maintain applied loads less than a few tenths of a nN, equivalent to a contact radius of ~ 0.2nm. This estimate is roughly equivalent to the radius of a single atom. In practice true atomic resolution is difficult and seldom obtained. Atomic resolution is, however, possible with SFMs. Usually, this requires operating in liquid environments which have been tailored to eliminate van der Walls and electrostatic tip-sample forces. Some have also reported atomic resolution in UHV with an Omicron STM/SFM.

By utilizing the capability of SFMs to monitor multiple signals simultaneously it is possible to image structures significantly smaller than these approximate contact areas suggest. Most notably, atomic scale corrugations can be seen on various surfaces, such as mica, in normal, lateral and error force images (Fig 3.4). There is no consensus as to the mechanism behind this fact but it is generally applicable to good SFM instruments: Figure 3.4 was obtained on the lab's Omicron STM/SFM in air.

Even though the vertical position of the cantilever can be adjusted reliably to 0.1 nm level precision, we cannot conclude that controlled applied forces of picoNewtons are possible. There are other sources of attractive forces between the tip and sample: electrostatic, van der Walls, and, in air, hydrostatic. These are discussed in section 3.3.2.

Given the calculated pressures of ~ 1GPa, it is not surprising that contact with

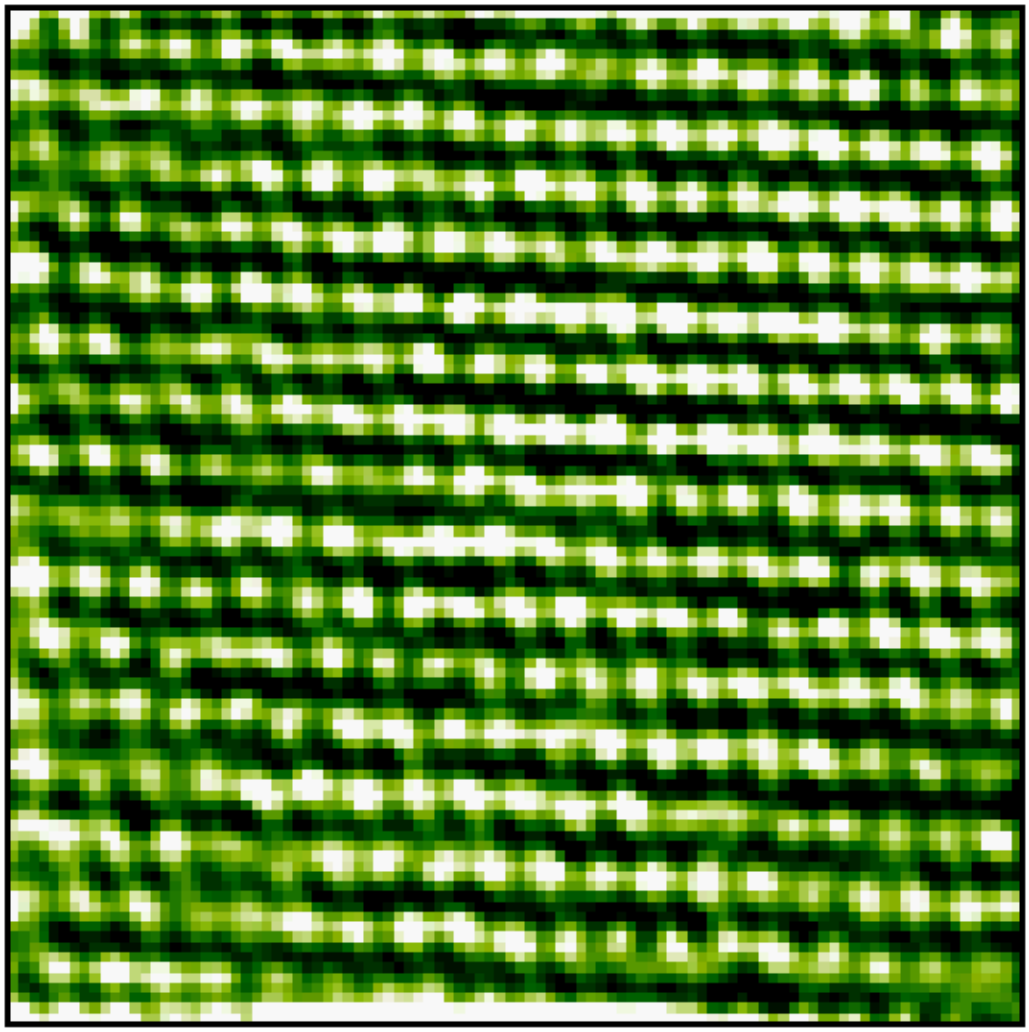

Figure 3.4

Atomic corrugation of mica, taken in air with the lab's Omicron STM/SFM. Atomic corrugation is not atomic resolution. Bumps do not necessarily correspond to individual atoms but only to average atomic locations. The piezo was not calibrated but comparason of mica and HOPG images taken with the Omicron with those taken with a calibrated SFM showed the same relative lattice constant difference between the two materials.

the surface can damage both it and the cantilever tip, especially when the items of interest on the surface are softer than the material used for the cantilever and tip. Most SFM tips used for Contact measurements eventually are damaged and become noticably blunt — as determined from a decrease in the effective lateral resolution of obtainable images. This is particularly true of the gold coated tips used for Contact I(V) measurements discussed in section 3.3.3. Such tips rarely survive three point contacts with a sample, much less repeated scanning across it. There is, of course, also damage to the surface at the nanoscale with repeated scanning of an area.[15] All these concerns limit the usefulness of Contact SFM. Luckily, there are many other methods available.

3.3 Extensions of Contact SFM

I briefly explain here the five additional methods of SFM I plan to use in this study, in order of increasing difference from Contact SFM.

3.3.1 LFM

The most straightforward modification of Contact SFM is Lateral Force Microscopy (LFM). The spring constants for a long thin beam are[16]:

$$k_{normal} = \frac{E}{4} W \left(\frac{T}{L}\right)^3 \tag{3.4}$$

$$k_{lateral} = \frac{E}{4} T \left(\frac{W}{L}\right)^3 \tag{3.5}$$

Using the known values for E, L, W, and T for common Silicon cantilevers (Ta-

bles 3.1 and 3.2), one generally finds that $k_{lateral}$ is one to two orders of magnitude greater than k_{normal}. However, the length of the beam is also one to two orders of magnitude less, resulting in lateral force sensitivities that are only about one order of magnitude below normal force sensitivities. In practice, LFM is usually used for qualitative measurements since calibration requires special samples designed for this purpose and since LFM has been found to resolve some sample features with more ease than Contact SFM. Specifically, atomic corrugation of hard samples and self-assembled monolayers (SAMs) is frequently easier to see in the lateral force signal.

3.3.2 Adhesive Forces

When the tip is brought into contact with the sample, its motion is not smooth. At some nonzero height above the sample, attractive forces between the tip and sample overwhelm the restoring force of the cantilever 'spring' and the tip 'snaps-to' the sample. If the tip is then retracted from the sample, it 'snaps-off' (Fig. 3.5). This behavior is due to electrostatic charges trapped in the tip or on the sample, electrodynamic or van der Walls forces, and, except in dry environments, capillary forces.

It is possible to quantitatively explain the van der Walls and capillary forces. Following Isrealachivili,[17] Chapter 14, it can be shown that for quite general cases, given certain approximations, the adhesion force between a sphere of radius R and a metal surface is $F = 4\pi R\gamma_s$ where γ_s is the surface energy per unit area of

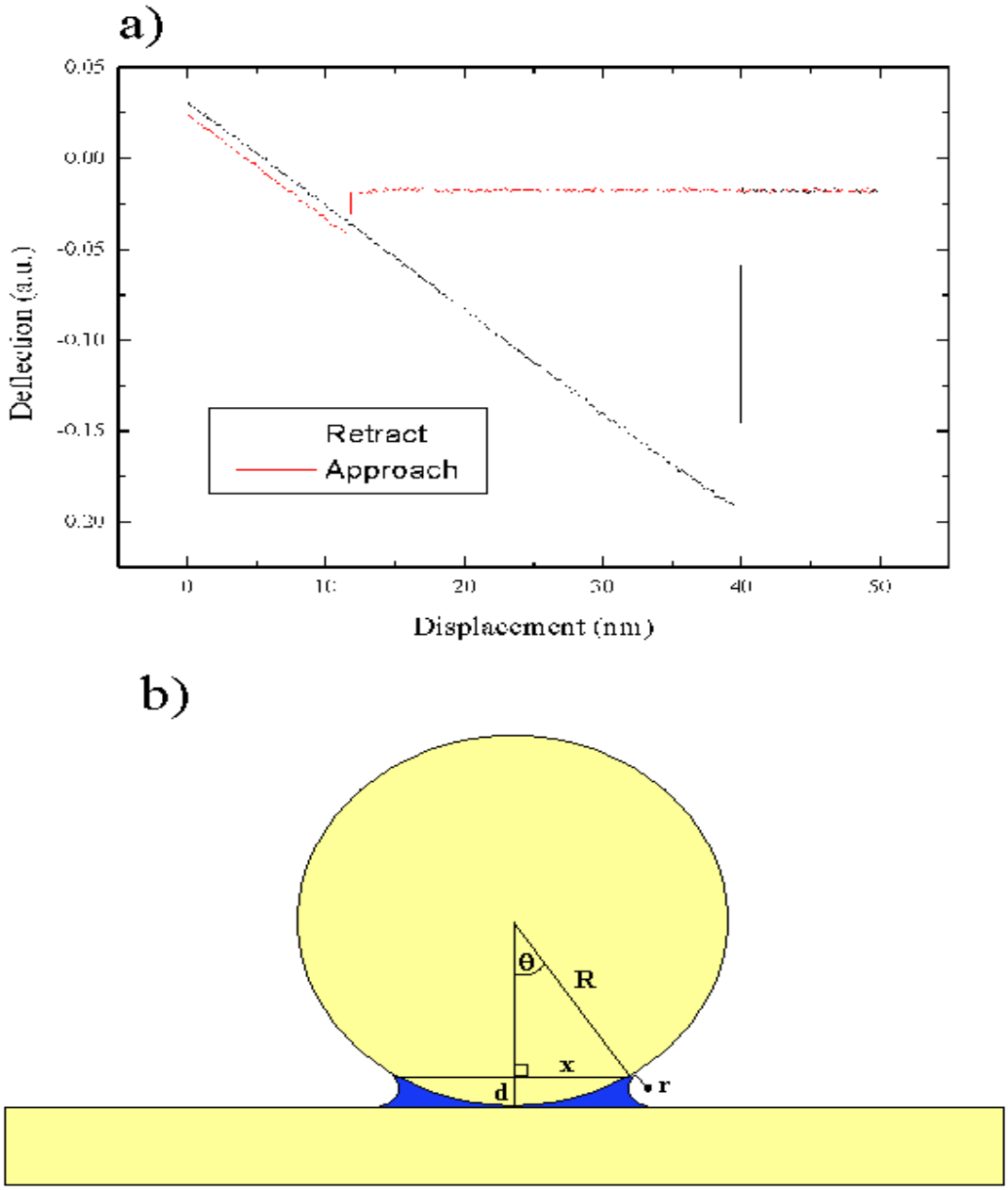

Figure 3.5

a) F(z) curve. The tip begins (right) far from the sample and moves in. vdW and electrostatic forces eventually overwhelm the cantilever restoring force and the tip 'snaps-to' the surface. Sample motion continues to a fixed set point and then reverses. Adhesive forces keep the tip in contact with the sample well past the 'snap-to' point. b) Adhesion model. The tip is assumed spherical and the sample planar. A circular contact area of πx^2 results. There is in addition an annular area of water around the edge of the contact reason which contributes to the adhesive force.

the sphere. Given R $\simeq$ 20nm and $\gamma_s \simeq 1000 mJ/m^2$ for gold, $F_{adhesion} \simeq 250nN$. Adhesion forces this high are very rarely encountered, even in UHV.

Liquids will condense from vapor on rough surfaces. At the nanoscale, most surfaces are rough, and most importantly, the immediate area of contact between the tip and sample can be considered to be a rough spot. The Kelvin equation gives the meniscus curvature (p/p_s is the relative humidity):

$$r_{meniscus} = \frac{\gamma_l V}{RT \log(p/p_s)} \tag{3.6}$$

where γ_l is the surface energy per unit area of the liquid, here water, R is the ideal gas constant, T is the temperature, and V is the molar volume.

For water $\gamma V/RT = 0.54nm$ and $r_{meniscus}$ varies from 0.5 to 2.5nm for relative humidities of 0.1 to 0.6, common for Purdue University air. Previous calculation of the contact area (Eqs. 3.3) shows that the water neck around the tip is approximately the same size or larger.

The associated pressure and force holding the tip and sample together can be estimated from the Laplace pressure equation

$$P = \gamma_l \left(\frac{1}{r_{tip}} + \frac{1}{r_{sample}} \right) = \frac{\gamma_l}{R} \tag{3.7}$$

with $\gamma_l = 73 mJ/m^2$ for water and $r_{tip} \approx 20nm$, P = 3.7MPa just in capillary pressure. Refering to Fig. 3.5 we can calculate the corresponding force, $F = \pi x^2 \gamma_l / r_{tip} = 2\pi r_{tip} d = 0.92nN$ in capillary adhesion.

In practice snap-off forces in average Purdue air are a few tens of nN, while snap-to forces are an order of magnitude less, and there is a great deal of variation between samples and scanning times. Electrostatic contributions on mica, which becomes highly charged on cleaving, can become so large that scanning is impossible and the tip cannot be retracted from the sample, corresponding to mN adhesive forces.

3.3.3 Contact I(V)

Here the cantilever is coated with a conductive material, frequently gold, tungsten carbide, titanium oxide, or titanium nitride.[18] An electrical connection is made between the cantilever and external equipment, and the tip is brought into contact with the surface as in normal Contact SFM.

If the conductive layer is strong, scanning may be done while a bias is applied between the sample and tip. One then monitors the current and constructs a "current image".[19] Alternately, the tip can be biased only at certain places and thereby cause changes to the surface at the nanoscale.

If the conductive layer is delicate, as it is for gold coatings, scanning almost instantly removes the gold from the end of the tip. In this case only point contacts are established and applied biases are ramped between two values.

Similar to the STM studies done here and elsewhere on alkylthiols, Barrena et al. have used this SFM method to study the alkylthiol SAM conductivity under various applied loads.[20] As little work has been done in this area, no general

theories have yet evolved.

However, this method's similarity to Scanning Tunneling Microscopy (STM), where a metal tip is held a few angstroms from the surface, usually in vacuum, and current is measured as a function of applied voltage, can be exploited.

Prof. S. Datta and his students have done much work on STM of molecular SAMs and developed some theoretical understanding.[21–23] Since I propose Contact I(V) studies of PM monolayers in Chapter 5, the simplest version of this theory (STM I(V) from α,α'-xylyl dithiol (XYL)) will be discussed.[21]

Consider the situation shown in Fig. 3.6. This is a representation of a SAM of XYL on an gold substrate. XYL is known to form a covalent sulfur bond to gold. The conductive STM tip in this case does not actually touch the XYL but hovers a few angstroms above it. Conventional wisdom suggests that I(V) data should be strongly asymmetric in this case for the following reasons.

The asymmetric bonding of the molecule to the tip and substrate leads to the assumption that the applied potential is dropped exclusively in the few angstroms between the tip and molecule. The molecule would be expected to strongly conduct as μ_2, the electrochemical potential of the tip, approaches the lowest unoccupied molecular orbital (LUMO). Similarly, for a negative sample, strong conduction would be expected as μ_2 approaches the highest occupied molecular orbital (HOMO). But the HOMO is a strongly coupled Sulfur-Gold bond and the LUMO is a weakly coupled benzene-ring orbital. So, much higher voltages would be expected to be necessary to achieve the same currents for LUMO conduction as for

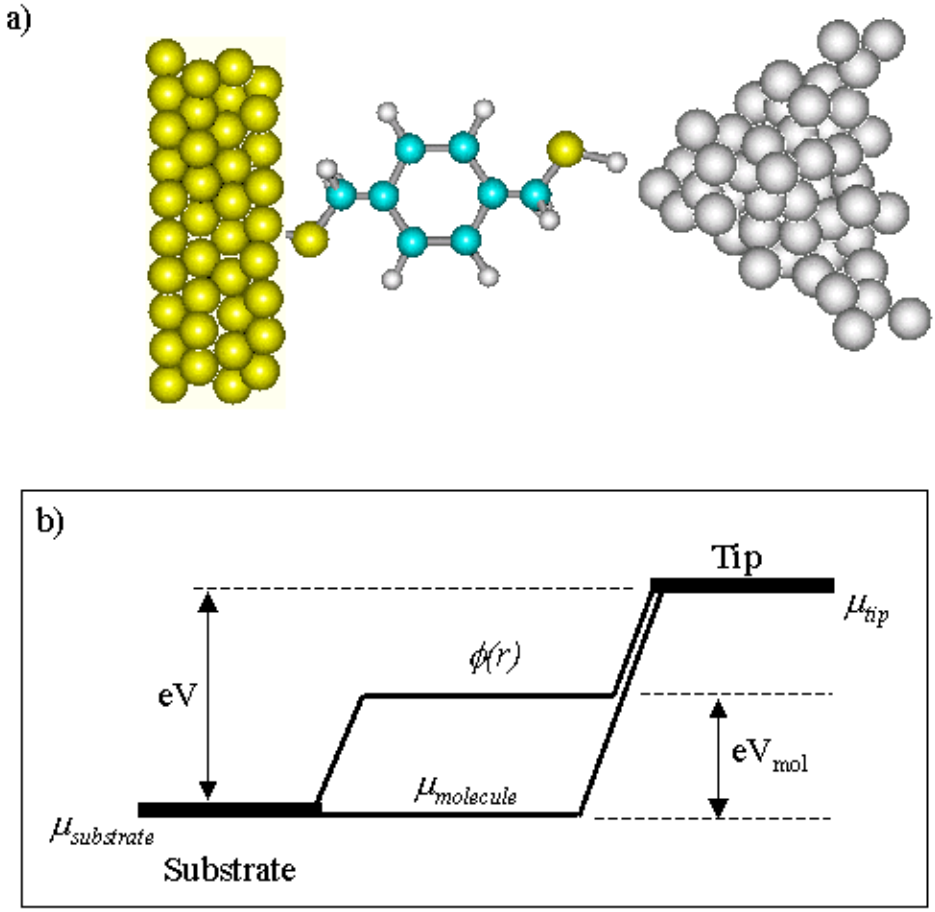

Figure 3.6

a) α, α'–xylyl dithiol SAM on a gold substrate with an STM tip in the tunneling regime. b) Voltage across the molecule. Both the chemical potential and the approximate electrostatic potential are shown.

HOMO conduction.

That this turns out not to be the case experimentally is the basis for the following theory. Assume that the molecular potential is not fixed at the level of the substrate. Assume instead that the molecular energy levels shift an appreciable degree in response to an applied field.

The conventional argument is that the electrochemical potential of the molecule is, because of the strong Sulfur bond, equal to that of the metal. But there are other potentials. The electrostatic potential ϕ(r) within an inhomogeneous conductor need not be constant. Specifically, it can be different in the molecule than it is in the gold. While the zero bias ϕ(r) is taken into account when calculating the HOMO and LUMO, the change $\delta\phi$(r) under an applied bias isn't.

Consider a parallel plate capacitor model. Since both the tip and substrate are metals, $\delta\phi(\mathrm{r}) = 0$ within them. Assume that no net charge enters the molecule, then $\nabla^2\delta\phi = 0$ and we have that the potential varies linearly along the molecule. The average potential in the molecule is then

$$V_{mol} = \frac{V z_{mol}}{L} \tag{3.8}$$

and to first order we assume that the energy levels of the molecule are fixed and let the sample move down by $\mathrm{eV_{mol}}$. Introducing $\eta = \mathrm{V_{mol}/V} \approx 0.5$ (since the tip is very close to the molecule) we have:

$$\mu_1 = \epsilon_F - \eta eV \tag{3.9}$$

$$\mu_2 = \epsilon_F + (1-\eta)\, eV \tag{3.10}$$

For conduction we need either μ_1 or μ_2 to be above (or below) E_h (E_l) or

$$eV > \min\left(\frac{E_F - E_H}{\eta}, \frac{E_L - E_F}{1-\eta}\right) \tag{3.11}$$

$$-eV > \min\left(\frac{E_F - E_H}{1-\eta}, \frac{E_L - E_F}{\eta}\right) \tag{3.12}$$

For the thiols for which this theory was developed, E_F is closer to the HOMO than the LUMO. The consequences for $\eta = 0.5$ are obviously that the conduction is through the HOMO for both positive and negative biases, thus I(V) data should be symmetric, which is experimentally shown.

This theory was developed for small thiol SAMs and explains the data well.[21] Several reasons to doubt the effectiveness of the foregoing theory for describing current through PM monolayers exist. PM consists of multiple species of molecules and contact area estimates indicate that more than one of these will be in contact with the tip during any data taking session. In this case we do not have a strong bond on one side of the molecule and a vacuum gap on the other. Both sides are in contact with gold. But are there bonds? On both sides or on one side only? The molecule of interest, bR, is orders of magnitude larger than the alkylthiols upon which the theory is based. PM is known to carry a large surface charge and

the little data collected shows asymmetric I(V) characteristics. Is this due to the surface charge or to HOMO/LUMO effects (thus contradicting the theory)? The size of bR could render calculation of theoretical I(V) curves problematic, thus making it difficult to say how well the theory quantitatively fits the data. Finally, is the Fermi level closer to the HOMO in bR and its associated lipids as is the case for the alkylthiols on which the theory is based? Nevertheless, this theory is the best we have at the moment. Its fate will have to await more data.

3.3.4 Noncontact SFM

Applying mega- and giga-Pascals to one's sample is not always desirable. It is also not necessary. The SFM can measure tip-sample forces without contact being established. While the dynamics of SFM cantilevers are not simple, for most purposes, a simple harmonic oscillator model suffices.[24] Consider a damped (due to tip-sample and tip-atmosphere forces) driven simple harmonic oscillator with equation of motion[25]:

$$\ddot{x} + 2\beta\dot{x} + \omega_0^2 x = A\cos(\omega_d t) \tag{3.13}$$

where $\omega_0 = \sqrt{\mathrm{k/m}}$, the resonant frequency for the non-damped, non-driven case, and $\beta = \mathrm{b/2m}$, the damping parameter. This non-homogeneous differential equation has a solution composed of a particular solution and a homogeneous solution, (the latter for the A = 0 case). The homogeneous solution is a product of an oscillatory term and an exponentially decaying term and so can be assumed zero

for steady state behavior.

The particular solution can be shown to be

$$x_p(t) = \frac{A}{\sqrt{\left(\omega_0^2 - \omega_d^2\right)^2 + 4\omega_d^2\beta^2}} \cos\left(\omega_d t - \delta\right) \tag{3.14}$$

$$\delta = \tan^{-1}\left(\frac{2\omega_d\beta}{\omega_0^2 - \omega_d^2}\right) \tag{3.15}$$

$$\tag{3.16}$$

We can also ask at what driving frequency the amplitude of x_p will be maximum. Taking the derivative of the leading term and setting it to zero gives

$$\omega_R = \sqrt{\omega_0^2 - 2\beta^2} \tag{3.17}$$

These three equations suggest two methods of measuring changes in the damping force (via β); both the amplitude and resonance frequency shift with β. Each method is used by one or more SFMs in the lab.

3.3.5 Electrostatic Force Microscopy

A variant of NC, EFM applies three signals to the cantilever: one to mechanically oscillate it, another to apply a time varying voltage to it, and a third DC offset voltage to it (Fig. 3.7). Otherwise the experimental setup, outside of the electrical connection between the sample and tip, is as in NC mode.

The voltage applied to the cantilever results in a component of the force signal oscillating at the frequency of the applied voltage. Lock-In techniques can be used

to measure this component and thereby infer the voltage difference between the cantilever and the sample. An important point to note is the use of the word 'cantilever' and not 'tip'. The cantilever beam cannot be ignored in this mode.[26,27]

Now consider the application of two voltages to the tip, V_{DC} and $V_{AC} = V_0 \sin(\omega_d t)$. The total force on the tip is

$$F_{total} = \frac{d}{dz}(U) = \frac{d}{dz}\left(U_{mech}(\omega_0) + U_{vdW} + U_{local} + U_{\mu}(\omega_0, \omega_d)\right) \tag{3.18}$$

due to mechanical driving, van der Walls, local electrostatic charges, and electronic equilibrium charge transfer because of work function differences between the tip and sample.

Let $U_{efm} = U_{local} + U_{\mu}$. Now assume the tip and sample are two plates of a capacitor, then $U_{efm} = \frac{1}{2}CV_{efm}^2$ where

$$V_{efm} = V_{\mu} + V_{local} + V_{DC} + V_{AC} \tag{3.19}$$

Then

$$\begin{aligned} F_{efm} \quad = \quad & \frac{1}{2}\frac{dC}{dz}\left((V_{local} + V_{\mu} + V_{DC})^2 + 2(V_{local} + V_{\mu} + V_{DC})V_0 \sin\omega_d t + \frac{V_0^2}{2}(1 - \cos 2\omega_d t)\right) \\ & + C\left(V_{local} + V_{\mu}\right)\frac{d\left(V_{local} + V_{\mu}\right)}{dz} \end{aligned} \tag{3.20}$$

We use Lock-In techniques to monitor the amplitude of the only component of this force that oscillates at ω_d,

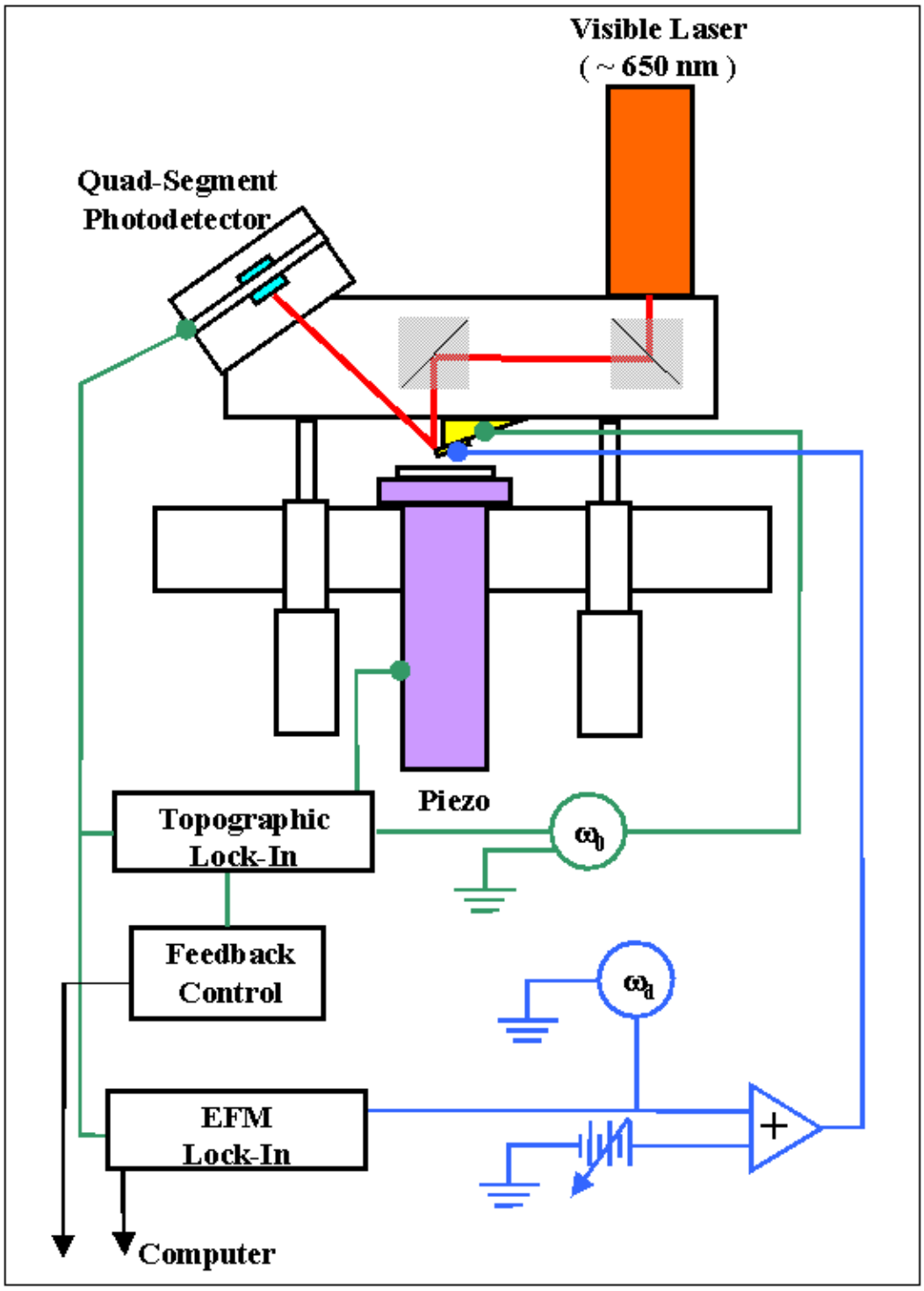

Figure 3.7

EFM NC-SFM circuit. Two feedback loops operate simultaneously and independantly. One maintains a fixed height of the tip above the sample, and the other, through the application of an AC and a DC voltage, measures the net electrostatic potential difference between the tip and sample at every point.

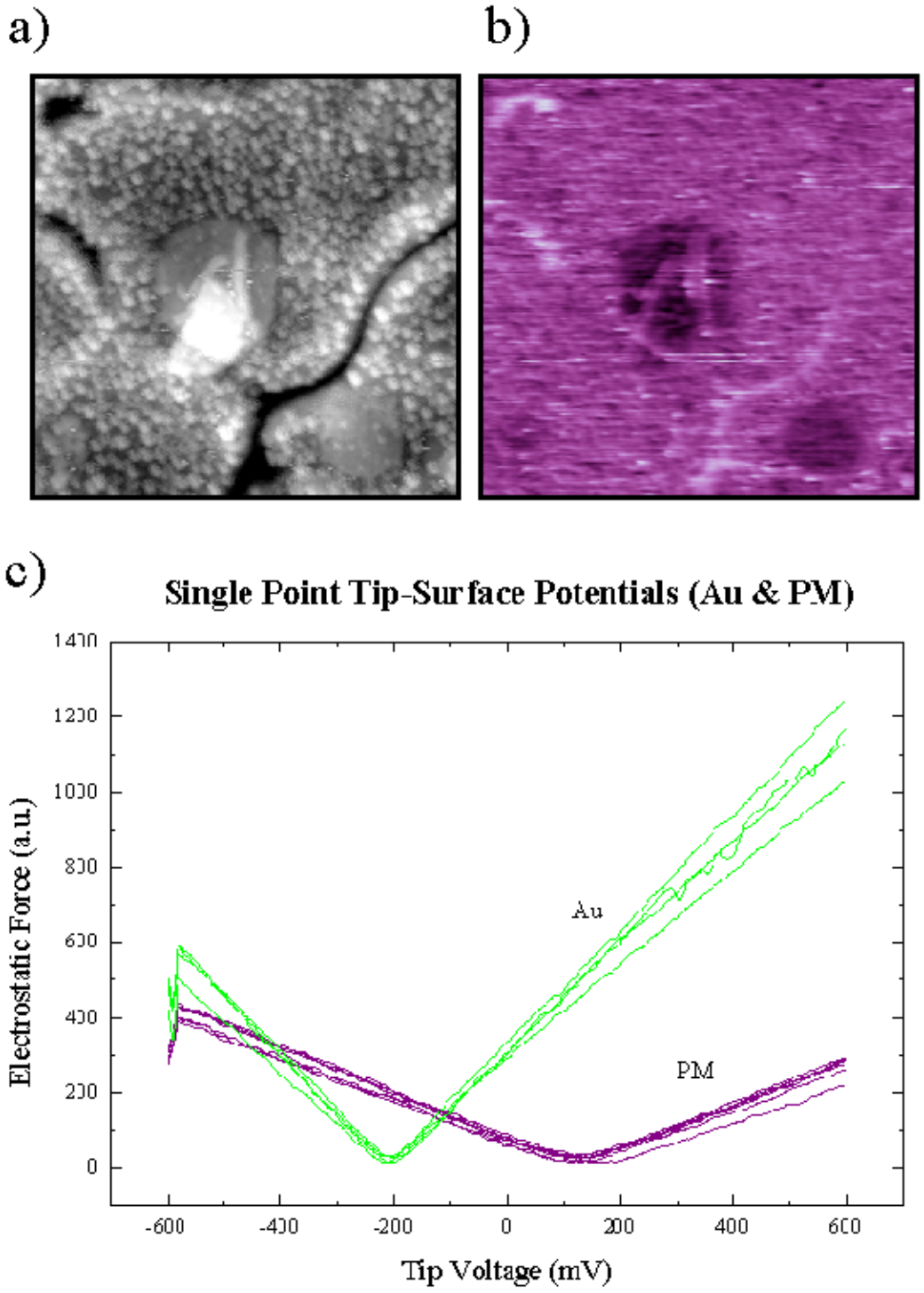

Figure 3.8

a) and b) Two dimensional, simultaneously acquired, topography and EFM images of PM on Au. Darker is more negative. The image is uncalibrated. (2.6 μm $\times$ 2.6μm $\times$ 80nm, 01260007.TOP and 01260007.CH2) c) Single point measurements over PM on Au. Uncertainties in the work function of the tip and the possibility of trapped charge on it render only the voltage difference between tip-Au and tip-PM meaningful.

$$A = \frac{dC}{dz} V_0 (V_{local} + V_\mu + V_{DC}) \tag{3.21}$$

We can use this for both 2D and 1D measurements. Operating a feedback loop to keep A = 0 (and hence $V_{DC} = -(V_{local} + V_\mu)$) and recording V_{DC} will give a map of $V_{local} + V_\mu$ at each point of the scan (Fig. 3.8 b)). Alternately, holding the tip fixed in X and Y and varying V_{DC} gives a single point measurement (Fig. 3.8 c)).

However, both Brian Walsh[26] and Steve Howell[27] have shown that the entire cantilever contributes substantially to the force between it and the sample due to the long range nature of electronic forces. Various responses to this problem exist. One can model the cantilever-substrate interactions and correct the results. One can adjust the sample coverage of PM to be uniform and close to 1.0M and comparing results with zero coverage measurements with the same tip. Attempts to do this have already partially succeeded. One can also attempt to decrease cantilever-substrate interactions so that they become negligable. I propose to attempt this.

Steve Howell has developed custom electronics to perform both point and two-dimensional EFM measurements. An estimate of the sensitivity of the system is 10 mV or less. These electronics are compatible with all SFMs in the lab.

3.4 SFM Apparatus

I anticipate using four different SFM instruments in the course of this investiga-

tion. The sequence of experiments I wish to undertake needs various environments and places certain requirements on interactions between the instrument and sample.

3.4.1 UAM

Figure 3.9a shows a commercial SFM from Nanotec Electronica, associated with the Universidad Autónoma de Madrid (UAM). The UAM uses a visible laser (650nm) beam-bounce detection method. It is easily modifiable and, through the use of a glass bell jar, can operate in modified atmospheric-pressure environments. Since 650nm is near the peak of the absorptance spectrum for bR, this instrument cannot be used to search for a photoactive dipole signal. Lateral and vertical resolution is limited to $\sim$ 1nm, making observation of the bR lattice by this instrument unlikely.

3.4.2 KFM

Figure 3.9b is an image of a UHV SFM designed and built here at Purdue[27] specifically to make EFM measurements. Cantilever position detection is fiberoptic-based infrared (1310nm) interferometry. Alternate gaseous atmospheres at variable, $\leq$ 1atm, pressures can be established. 1310nm is far beyond the sensitivity range of bR,[10] thus this instrument can be used in attempts to measure the dipole activity of PM. Lateral cantilever motions cannot be detected. Lateral and vertical resolution is limited by the use of UAM control electronics to $\sim$ 1nm, similar to the UAM.

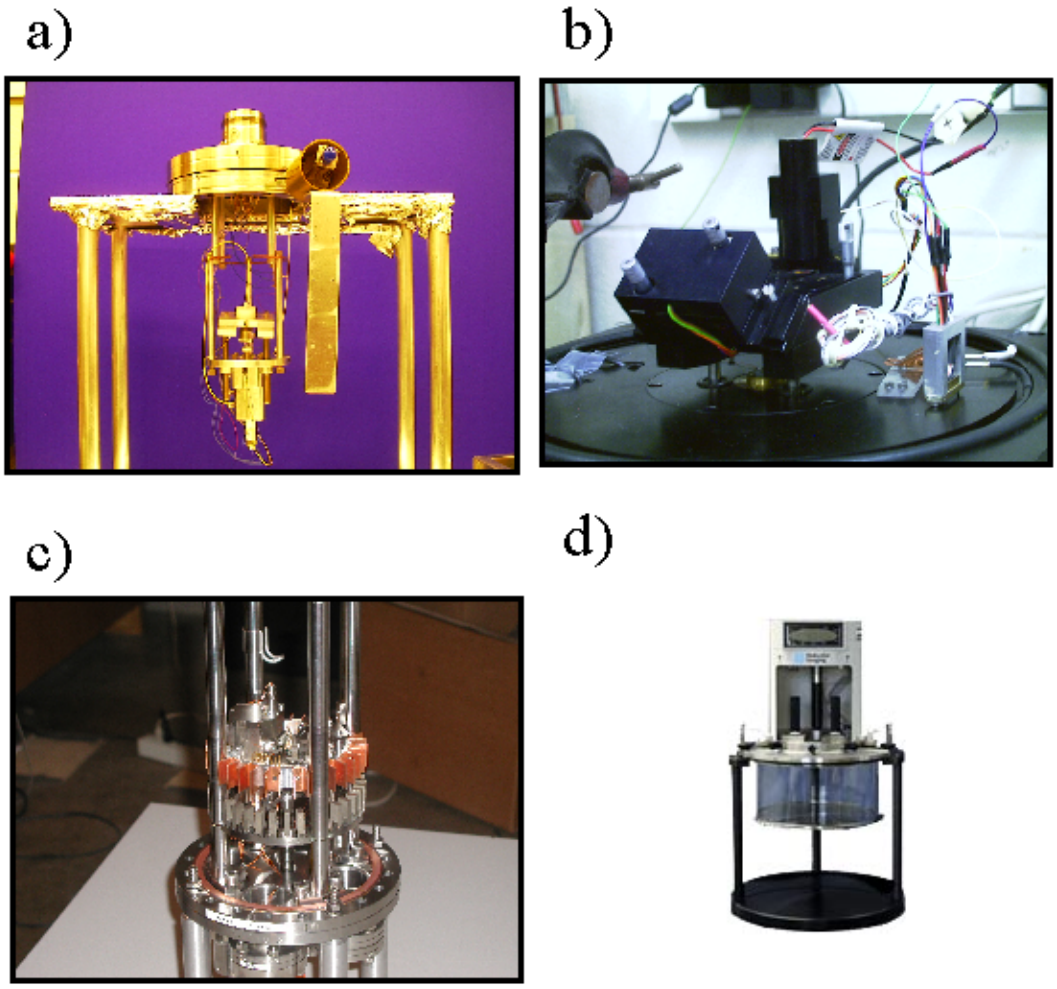

Figure 3.9

The labs SFMs. a) The UAM, operates in air with a visible laser. b) KFM: UHV, infrared laser. c) Omicron: UHV, infrared laser, much better lateral and vertical resolution than a) or b). d) MI: Air, visible laser, operates under water. Also high resolution.

3.4.3 Omicron

Figure 3.9c shows the lab's latest UHV system, a commercial SFM/STM from OMICRON Vakuumphysik, GmbH. Operating with an infrared beam-bounce detection method, it is suitable for dipole activity measurements. The Omicron should be more than capable of achieving atomic scale resolution (lateral and vertical) and will be utilized for the task of imaging individual bR within the PM lattice. It is hoped that the current state-of-the-art image (resolution of individual α-helices) can be duplicated in UHV.

3.4.4 MI

The latest air SFM acquired by the lab is a commercial SFM capable of operating in liquids or in air (Fig. 3.9d). It uses a visible laser beam-bounce detection method making it unsuitable for dipole activity measurements. Along with the Omicron, the Molecular Imaging, Inc. (MI) SFM should be capable of resolving the bR lattice in a liquid environment. Also capable of operating under controlled environments, it is preferable for some EFM and I(V) measurements.

Table 3.2

Physical Dimensions and Properties of Typical Contact and Non-Contact Cantilevers

	Contact	Non-Contact	Units
L	450	225	μm
W	50	38	μm
T	2	7	μm
H	10	10	μm
k_{normal}	0.2	48	N/m
$k_{lateral}$	125	1400	N/m
ω_0	13	190	kHz

4. Preliminary Results

While there is a great deal of research on PM, little of it is SPM-based. Most studies have concentrated on elucidating the properties of the (complicated) photocycle. However, some results are relevant to our research.

The photocycle has been shown to change with relative humidity[28] and the net electrostatic surface charge on PM in solution has been shown to be pH dependent[10] and even to change sign; i.e., sometimes the intracellular side is net negative and sometimes net positive.[29] Net electrostatic surface charges of a few electrons per bR have been measured by different means and different authors as well as the quantum efficiency of bR.[9] The absorption spectrum has been well established.[10]

Various authors have resolved the bR lattice in PM with effective resolutions ranging from 1.1nm[30] to subnanometer lengths,[8] the latter being sufficient to show the individual α-helices. Recently, F. Oesterhelt, et al. successfully used genetically modified bR and a gold-coated SFM tip to extract a single bR molecule from a PM patch and record the forces as the protein unfolded.[31] PM appears to crack when dried on mica[3] but not on gold or when kept in solution. Whether this is due to electrostatic attractions, covalent bonding to the surface, or some other mechanism is unknown.

Various sample preparation methods other than simple deposition-and-wash have been shown to produce submonolayer coverages. Jin-An He, et al.[32,33] constructed multiple layer sandwiches of PM and a charged molecule used to glue them together. AC Photoactivity was shown to persist. Genetic modification of bR has been shown to encourage covalent bonding of PM to gold substrates.[34] A method I propose to use, electric field sedimentation, has been used to control the surface coverage by use of an externally applied electric field which acts on the net electrostatic dipole of isolated PM patches.[11] This allows one to choose which side, exo- or intra-cellular, of the PM lays down on the substrate.

4.1 Preliminary Results

Preliminary measurements have been made to test for capability. PM has been deposited at sub-monolayer coverages on various substrates and been imaged in various SFM modes on multiple SFM instruments. A small set of I(V) data has been obtained.

4.1.1 Deposition and Location of PM on Various Substrates

PM has been deposited on gold and HOPG substrates at coverage levels between 0.01M and 0.4M. Higher levels, while obtainable, suffer from excessive overlap of individual PM patches, thus complicating any but topographic analyses. A suspension of PM in deionized water, prepared by our collaborators, R. Birge and D. Marcy at Syracuse, was used for all samples prepared here at Purdue.

Sample preparation consists of depositing a drop of PM solution on a recently

flame-annealed gold substrate. The drop is then either allowed to evaporate under light vacuum (house vacuum, absolute pressure unknown) or, after sitting for a period of time, is rinsed away with deionized water (DI water) and dried under a flow of dry nitrogen gas.

Fig. 4.1a shows some typical topographic images of PM on Au substrates. PM patches are seen to be a few hundred nanometers in diameter and roughly circular. Frequently they display what apepar to be wrinkles. In the lower right there are what appear to be overlapped patches. Additionally there are much smaller objects on the gold surface. Since their heights are frequently greater than PM it is not clear what these are. They are always present after application of PM solution to gold substrates.

Samples made by allowing the PM solution to evaporate (Fig. 4.1b) produce coverage levels varying from 0.1M to ~100M over a distance of a few mm. The largest range SFM we have can move the sample laterally $\sim 100\mu$m and typical scan sizes are 3–10μm. For all but EFM measurements such a slow variation in coverage is effectively equivalent to constant coverage.

Other authors have imaged PM with SFMs.[1–4,8,30,35–39] Their PM patches were equivalent in size and shape to those shown in Fig. 4.1. Of note in the literature is a large variation in measured surface heights of PM (4–11nm) deposited on various surfaces. It has also been reported that isolated PM is charged to a few hundred mV.[4] As discussed later in this section I, along with Steve Howell, have measured similar voltage differences between isolated PM patches and the surrounding gold

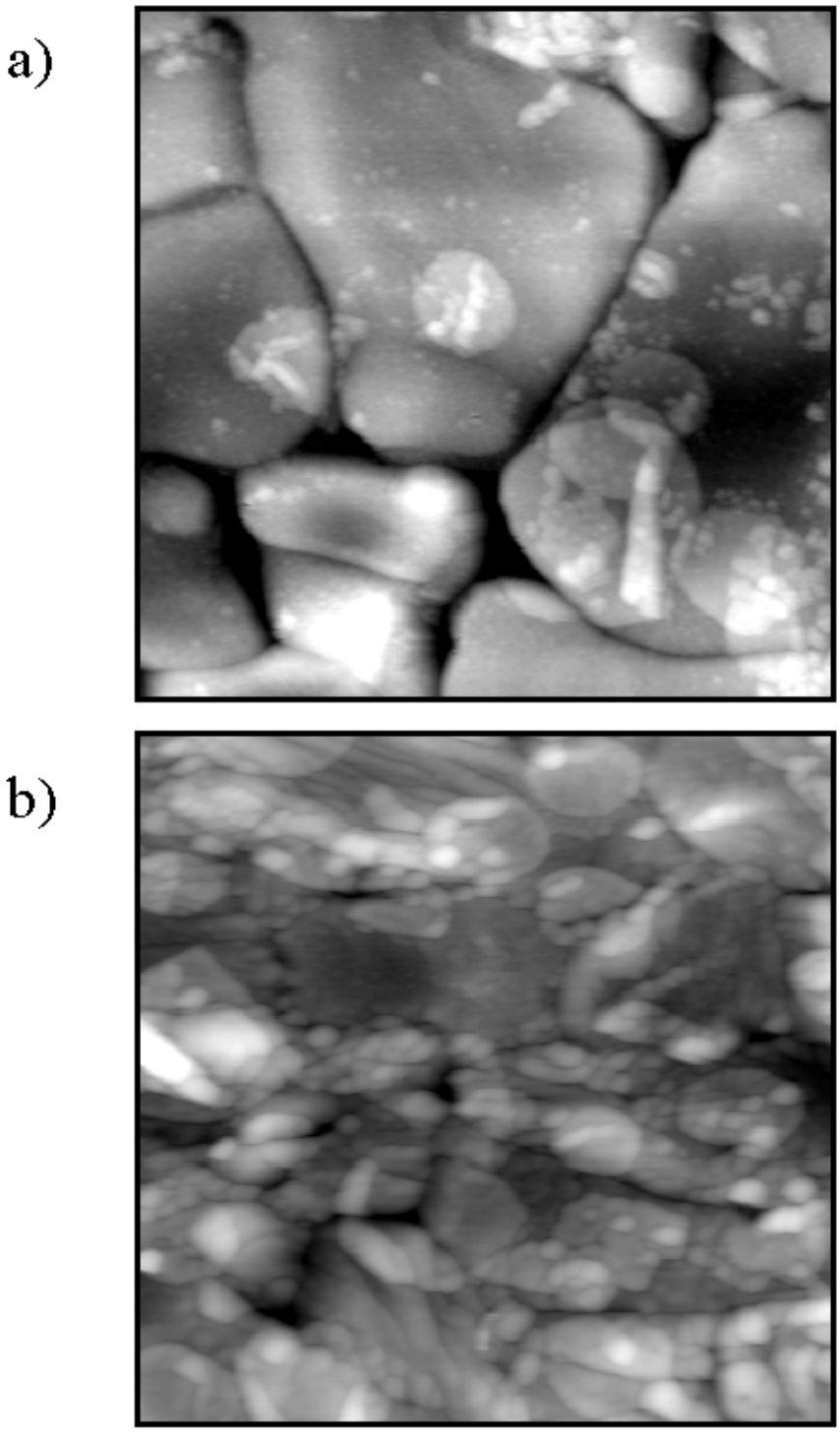

Figure 4.1

PM on Au. a) Multiple PM patches are visible. Some are isolated, some apparently wrinkled, and some overlapped. Heights are $\sim$ 5nm (3.0μm $\times$ 3.0μm $\times$ 31nm, 12039920.TOP). b) Higher coverage of PM on gold (3.0μm $\times$ 3.0μm $\times$ 35nm, PM-PUAu_001_000713_0009.f.TOP).

substrate. It is not clear if we have measured with respect to the same voltage zero point.

PM on Au can be distinguished from the substrate by topography, adhesion, or EFM. Many samples have been investigated. As a result the nature of the PM solution provided by D. Marcy has been clarified and the ability to locate PM on various substrates has been demonstrated.

4.1.2 I(V) of PM on Au

PM was deposited on a flame annealed gold substrate. Thermal evaporation was used to deposit $\sim$ 5nm Ti followed by $\sim$ 30nm Au on a small number of NC cantilevers. These were used to image, in NC mode, the PM on Au substrate in the UAM SFM. Due to the delicate nature of the Au-Ti coating, care was taken to minimize accidental, but frequently unavoidable, tip-sample contact. Upon locating an isolated patch of PM, the cantilever mechanical oscillation was stopped and the tip was brought down into contact with the PM patch on the surface. Single point I(V) curves were recorded. I did not scan the tip for fear that this would remove the gold coating. After I(V) data was collected on PM, the tip was raised out of contact with the surface, an NC image was made to verify that piezotube hysteresis had not caused the tip to drift out of contact with the PM, the tip was moved laterally to a known PM-free gold grain, and the tip returned to contact. More I(V) data was collected. Once more the tip was removed from contact with the surface, an NC image was made to verify position, the tip was

moved to another PM-free zone and brought into contact. Another set of I(V) curves were recorded. The process of collecting I(V) data from various locations on the gold surface continued until the I(V) curves became nonlinear.

The only method we have of testing the quality of the gold coating at the end of the tip is to bring it into contact with a metal substrate. But the contact forces involved (nanoNewtons over a few tenths of a square nanometer), frequently damage the very coating being tested. It is rare, in practice, to see a gold-coated tip produce Ohmic contacts for more than three encounters with a metallic surface. The tips we use are either Silicon with an outer oxide layer or Silicon Nitride. Both yield semiconducting I(V) curves when bare.

This delicacy of the tip set the above procedure for taking I(V) data on PM. The first data is collected on PM over gold (henceforth PM-Au). Whether this can be reliably interpreted as being from a gold electrode in contact with PM must be tested after the fact since the tip is unlikely to survive the test. The second set of I(V) data, on gold only (Au-Au), hopefully proves linear, i.e. Ohmic. From this I hypothesize that there was an Ohmic current path all the way to the end of the tip in the previous I(V) data on PM. Once the tip has been in contact with an gold surface it is suspect, so repeated tests are done until semiconducting I(V) data is observed (Si-Au). Hopefully, this is significantly different from the PM data. If it is and if the Au-Au data is linear, then I conclude that the PM-Au data really was due to a single layer of PM sandwiched between two metal contacts.

A representative data set is shown in Fig. 4.2 along with a schematic of the

state of the tip during each I(V) collection. The PM-Au curve shows interesting features: It is not symmetric about zero bias, it is nonlinear and significantly more resistive than the Au-Au contact (Fig. 4.3). To my knowledge, this is the first time that I(V) data have been collected through a single layer of PM.

We can use the I(V) data for the Au-Au case to estimate the contact area from the equation for the Sharvin conductance of a metal-metal point contact[40]:

$$r = \sqrt{\frac{4\rho l G_S}{3\pi}} \tag{4.1}$$

For bulk gold l is well known to be $\sim$ 40nm, but recent results[40–42] indicate that for nanometer sized contacts l could be as low as 4nm.

Given $\rho_{\mathrm{Au}} = 2 \times 10^{-8}\Omega$m, (from Fig. 4.2b) $G_S = 0.6 \times 10^{-3}(\Omega\mathrm{m})^{-1}$, and $l \simeq 10$nm we find that r = 0.2nm. Comparing this with the previous estimation (Section 3.2) we see that both methods reach essentially the same conclusion to within a factor two.

4.1.3 EFM

Electrostatic forces between the sample and the tip were also measured. Various samples of PM on gold were investigated. Fig. 3.8 shows an EFM image and associated, simultaneously acquired, topographic image (processed to show the PM clearly). The absolute EFM scale is unknown and, as discussed in section 3.3.5, convolution with the cantilever would have reduced the measured potential difference from the actual value.

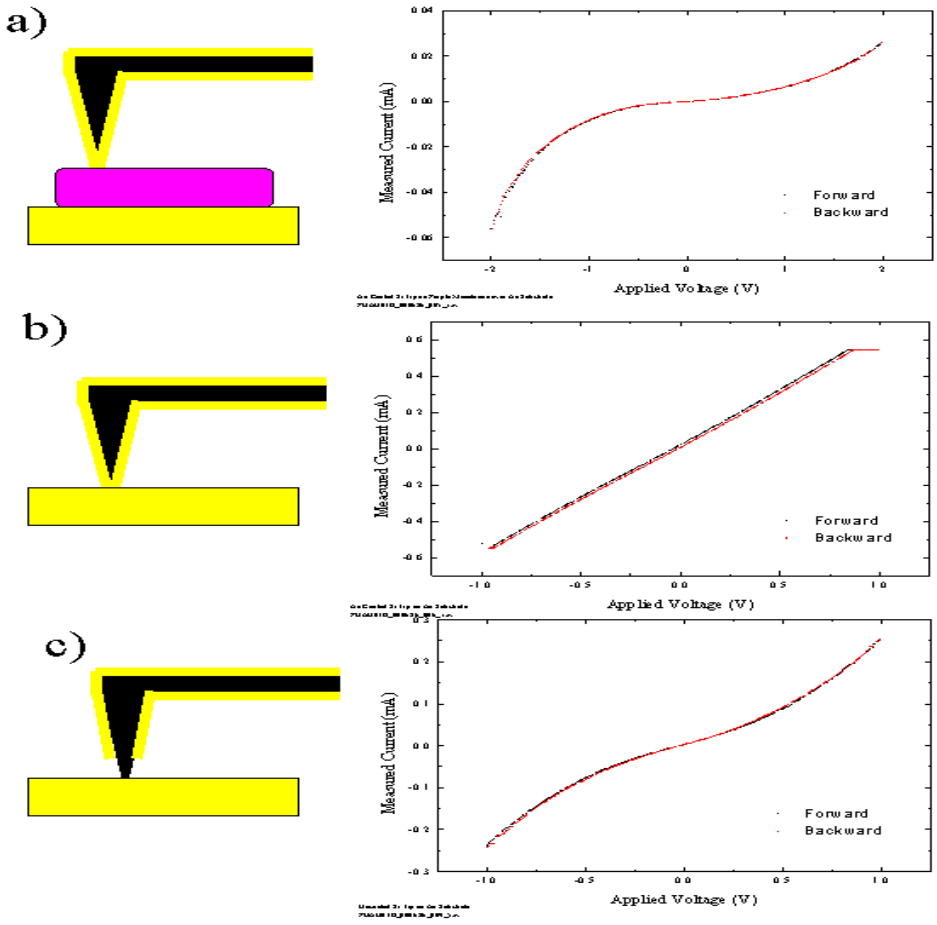

Figure 4.2

Contact I(V) Methodology: The sample is first imaged in NC mode and a suitable PM patch is located. Then a) cantilever oscillation is stopped, the tip is brought into contact with the PM, and the voltage is varied from V_{min} to V_{max} and back again. b) The tip is retracted and another NC image is made to verify negligable hysteritic drift. The tip is brought back into contact *on gold* this time and another I(V) data set is acquired. The linear I(V) suggests that the tip still has an gold coating. c) The tip is retracted again and returned to contact. I(V) data proves non-linear from which it is inferred that the gold coating was removed during the last retraction.

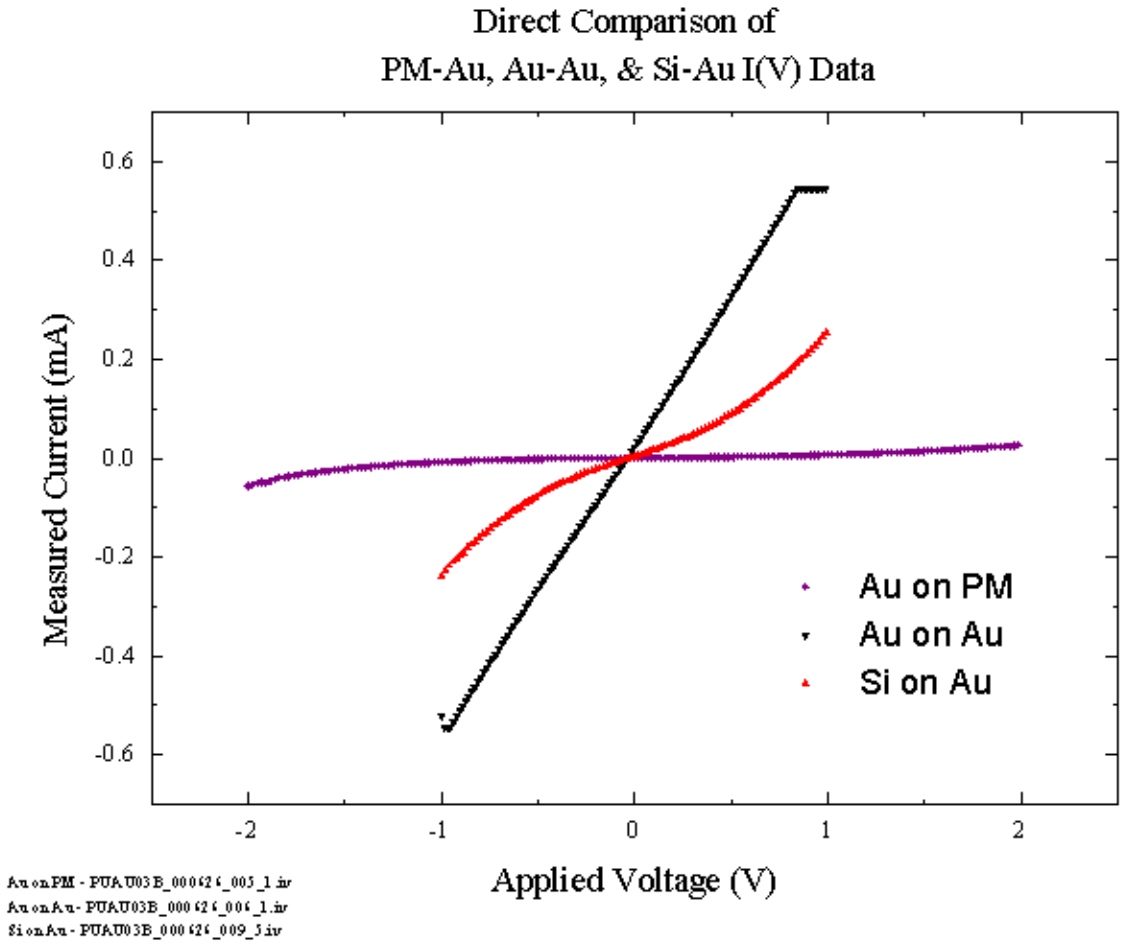

Figure 4.3

Contact I(V) Comparison: All the data from the previous figure is shown here on the same scale. The large resistivity of PM is now obvious.

Single point EFM measurements (Fig. 3.8c) where the PM covered the surface to a depth of a 10 to 100μm over a lateral diameter of $\sim$ 1cm show a 300mV potential difference between PM and bare gold. Most bacterial membranes are charged in solution and levels of a few hundred mV are reasonable.[43]

4.1.4 Adhesion

Combined topographic and adhesion images of PM on gold have also been acquired. Fig. 4.4 shows a measurable difference in adhesion between PM and gold in air. Darker colors correspond to lower adhesion. These images demonstrate the ability to identify biological membranes on surfaces from their hydrophilicities.

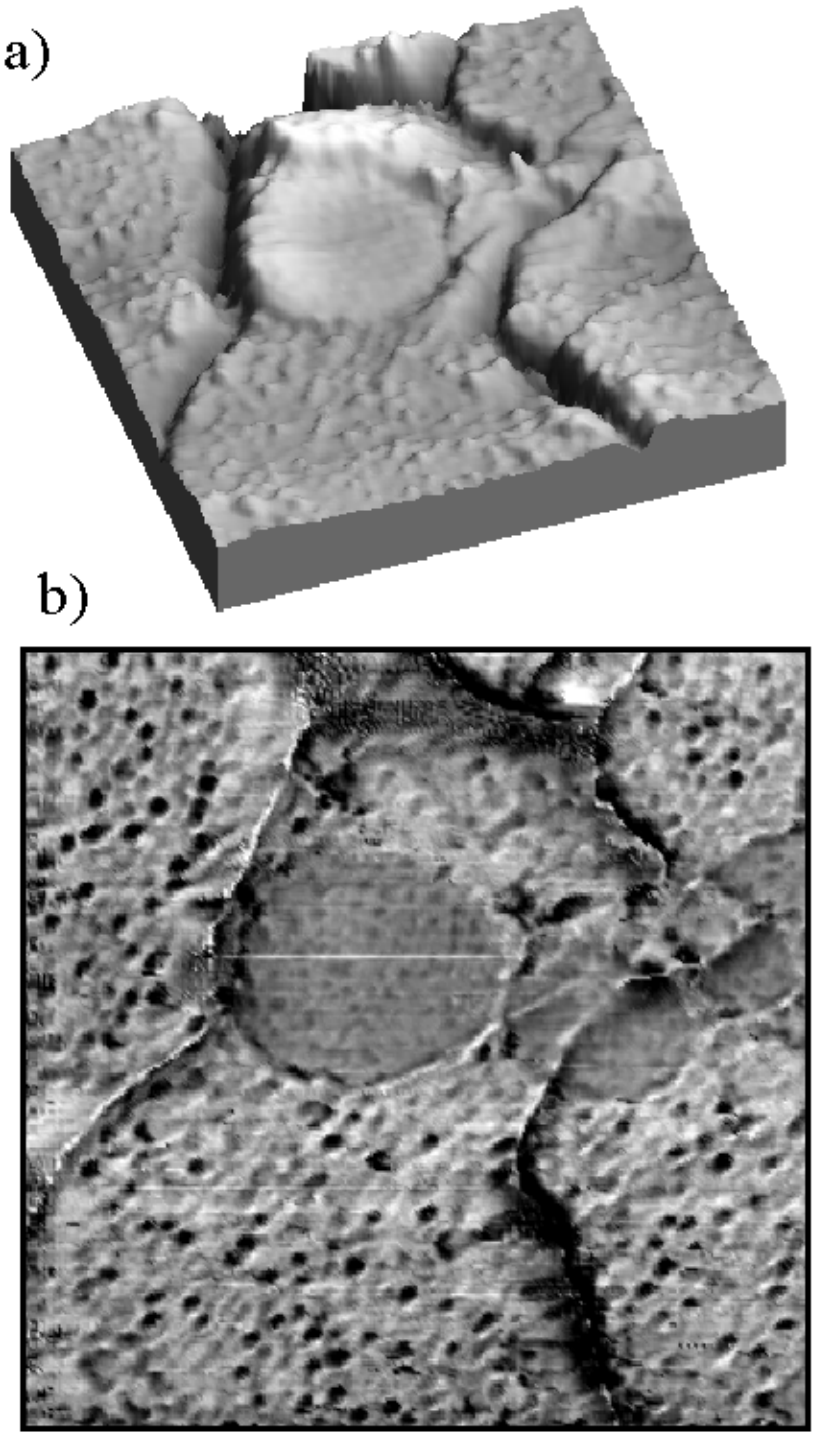

Figure 4.4

Simultaneously acquired topography (a) and adhesion (b) of PM on Au. Adhesion uncalibrated. (1.0μm $\times$ 1.0μm $\times$ 92nm, 99122816.TOP and 99122816.PAR)

5. Future Plans and Summary

Measurements to date have served only to demonstrate certain capabilities; to distinguish PM from the substrate in various ways, to show a net charge in air, to show distinguishable contact I(V) characteristics, and to deposit PM on various substrates in submonolayer coverages. In depth studies must still be undertaken.

5.1 Sample Preparation and Types

5.1.1 A Proliferation of Types

Almost all data collected so far at Purdue University has been of PM on Au. If PM is to be integrated into semiconductor devices we obviously would prefer to deposit it directly on Si and GaAs. Other authors have shown both a humidity and pH dependence to the photoactivity of PM on substrates in solution. Bringing proteins into contact with metals tends to cause denaturization and bR has proven sensitive to configural changes.[9]

I propose to address all of these issues. We have access to and experience with both Si and GaAs substrates through long term collaborations here at Purdue. Deposition of PM on these substrates via the evaporation method should be straightforward. We have the ability to control both humidity and pH in solution with the new MI SFM. Insulating the PM from the metallic substrate by

a conductive SAM which does not cause configurational changes in the bR could be necessary to observe a photoactivated potential change of PM. The Lab has developed the capability to deposit SAMs of various molecules on Au substrates.

Finally, if attempts to detect a change in surface potential due to light activation of the bR in PM are successful, control of the intermediate SAM (type and height) could yield interesting EFM results. I therefore propose attempting to deposit PM on top of a SAM and on both Si and GaAs.

5.1.2 A Proliferation of Preparation Techniques

Current techniques of depositing PM have drawbacks; I judge at least one to be potentially serious for EFM measurements. Allowing the PM solution to dry on the sample results in transfer of much of what is in the solution to the surface. It also results in PM coverage changes which may not be negligible over the $\sim 200\mu$m length of the cantilever. Additionally, the bR molecules in PM are not symmetric across the plane of the lipid bilayer. The intracellular side is different, in both structure and net charge density, from the extracellular one. Finally, PM consists of two different molecules: lipids and bR. As previously estimated, the contact area for I(V) curves is greater than a single bR. Studies of PM are therefore studies of both molecules simultaneously.

At this time, depositing the lipid bilayer which holds the bR in the PM by itself appears to be a difficult problem, as isolating the particular lipids has never been done. We must, therefore, live with the complex of molecules that is PM.

Other authors have demonstrated the ability to choose which side of PM adheres to the substrate by applying a net voltage between the substrate and the PM solution.[11] A similar technique may allow us to avoid evaporating the PM solution while still achieving $\sim$ 0.3M coverage. I further propose to attempt to increase our ability to control the coverage percentage and choose which side of PM is attached to the substrate using electrostatic deposition based on an externally applied electric field. By varying the strength and time of application of this field it may be possible to control the amount of PM deposited.

Finally, many groups have demonstrated the ability to deposit molecular monolayers on substrates in patterns with minimum feature scales $\sim$ 100nm and maximum feature scales $\sim$ 1mm. Such 'Stamp Pad' techniques have been demonstrated here at Purdue. I propose attempting to control the locations of deposited PM patches using stamp pad techniques.

5.2 Enhanced and New Techniques

5.2.1 Improve lateral resolution of EFM

The convolution of sample and cantilever limits the usefulness of EFM for Ångstrom and nanometer scale investigations. Other groups have reported increased lateral resolution in NC SFM by attaching a carbon nanotube to the end of the tip.

Carbon nanotubes are far more popular research subjects than bR. There is no space, nor need, to describe here their properties to any great degree. For my

purposes they are merely very small (2–100 nm diameter), very sturdy, very thin (1–10μm long) objects which we have previously been able to mount on the tips of SFM cantilevers. This attachment effectively moves the tip of the cantilever further from the cantilever itself.

Moving most of the mass of the tip and all of the cantilever away from the sample by a few microns should reduce convolution effects, especially for very disperse PM depositions. For EFM measurements to work, however, essentially all of the potential applied to the tip must reach the very end of the nanotube closest to the sample.

Only $\sim$ 30% of nanotubes are metallic (the others are semiconducting). The method used at Purdue to mount nanotubes requires the use of ropes of multiwall carbon nanotubes (MWNTs) — essentially an aglomeration of smaller tubes. Frequently some of these tubes are not continuous throughout the entire rope. Thus one cannot tell what percentage, if any, of the voltage applied to the cantilever actually reaches the tip of the MWNT.

A solution, proposed by Dr. Elton Graugnard while a graduate student in our lab, is to coat the MWNT and the cantilever with Au. We have the equipment to do this. I propose doing so and using these tips to obtain better resolution EFM images of PM, perhaps resolving the bR lattice.

5.2.2 NC STM

Others have shown the ability to combine STM with NC SFM and to simul-

taneously measure both topography and tunneling current (henceforth NC-STM). This technique may also allow higher lateral resolution due to the nonlinear nature of the tunneling current.

This type of SPM technique has never been used in our lab. I propose using NC-STM to attempt to measure tunneling currents through PM.

5.3 New and Improved Measurements

5.3.1 Alternate Methods of bR Lattice Resolution

Other authors have reported resolution of the bR lattice in PM, some going so far as to show individual α -helices. This work has been done in solution and in contact mode. I propose to attempt to resolve the bR lattice with other techniques.

LFM has been used to resolve molecular lattices of alkylthiol SAMs.[44,45] Given bR's larger size, I suspect LFM could resolve the bR lattice as well.

Other groups have reported enhanced lateral resolution with the addition of a Carbon Nanotube to the end of the SFM cantilever tip. I propose to construct such 'nanotube tips' and attempt to resolve the bR lattice in air, dry N2, and UHV.

A variant of the EFM measurements described here has been performed on PM in various solutions.[4] No one has yet made such measurements in air, N2, or UHV. Since these measurements present little difficulty, I propose to study environmental effects on PM charging.

Finally, I propose additional study of contact I(V) characteristics of PM on

various substrates. To date, due to a scarcity of conductive SFM tips, only a few I(V) data sets have been acquired. An in-house evaporator should soon be available to rectify this difficulty. A great deal of effort has been expended in the lab to study the I(V) characteristics of SAMs of small molecules on Au substrates. Because PM is composed of a complex of molecules, one of which is orders of magnitude larger and possessive of more properties (photoactive dipole, large surface charge) than anything yet studied by the lab, it presents an opportunity to extend the range of the theories developed for I(V) characteristics of molecular SAMs. Furthermore, other authors[20] have demonstrated variations in I(V) data on SAMs with applied force using an SFM. I propose to do the same with PM.

5.3.2 Detect photoactivated dipole via EFM

Many authors have demonstrated detection of photocurrents and photovoltages from illuminated PM. Spectroscopic methods have been used to measure the dipole strength.[9,29] No one has yet directly measured the voltage change between excited and unexcited PM monolayers. I propose to use the EFM techniques developed here at Purdue University to attempt to measure the degree of activation of the dipole in bR.

Since the dipole is only photoactivated, illuminating the PM with light whose frequency is at the peak of bR's absorption spectrum should produce a voltage contrast between it and the unilluminated state. If this voltage difference proves possible to detect, EFM would then provide a non-invasive, high resolution method

of determining bR photoactivity.

To date, EFM studies have concentrated on static voltage differences of large, multimicron-scale features. The ability to measure, with potentially tens-of-nanometer resolution, photoactivated dipole charges would open to investigation a host of additional systems. Technologically, the ability to produce robust devices incorporating PM depends on the ability to gauge the quality of the bR proteins themselves. While other, large scale tests exist, nanoscale engineering would benefit from nanoscale testing of components.

Preliminary tests have shown mixed results. Definite voltage contrast exists between isolated PM patches (and multilayer coverings) and bare gold, but attempts to witness photoinduced voltage changes have failed. Sample quality issues render these tests inconclusive. They do, however, raise the issue of whether or not any effect should be observable. The absolute magnitude of the dipole appears, from the literature, to have been of little interest. Further research must be done to determine if anyone has measured it or measured some property from which it can be deduced.

Therefore, at this time, it is not clear that any signal should be observed. Sensitivity measurements were conducted over complete monolayers, the entire cantilever was over the relevant molecule. The measurements I propose would be over isolated PM patches and the PM-cantilever interaction will be smaller, possibly negligible. Furthermore, all previous measurements of bR photoactivity have been performed in solution or with many hundreds if not thousands of PM

layers. It is not known to what extent bR is still photoactive when deposited on a substrate and it may be that too few of the bR still fire to produce a measurable voltage difference.

5.4 Summary

In summary I propose to investigate the electrical conductivity of single layers of PM under various atmospheric conditions and as deposited on various interesting substrates. Further I wish to investigate dipole activity of PM with SFM techniques and, finally, to attempt to improve the lateral resolution of the EFM technique.

ACKNOWLEDGMENTS

I thank Dr. R. Birge and Dr. D. Marcy of Syracuse University for providing the Purple Membrane for this study, instructions for it's proper handling and storage, and the creation of the initial set of samples. I thank my advisor, Ron Reifenberger for his invaluable guidance during the course of this work.

BIBLIOGRAPHY

BIBLIOGRAPHY

1. Hans-Jürgen Butt, Biophys. J. **60**, 1438 (1991).

2. Hans-Jürgen Butt, Biophys. J. **60**, 777 (1991).

3. Hans-Jürgen Butt, C. B. Prater, and Paul K. Hansma, J. Vac. Sci. Technol. B **9**, 1193 (1991).

4. Hans-Jürgen Butt, Biophys. J. **63**, 578 (1992).

5. Reginald H. Garrett and Charles M. Grisham, *Biochemistry*, Saunders College Publishing, 1999.

6. F. T. Hong, Prog. Surf. Sci. **62**, 1 (1999).

7. Walther Stoeckenius, Richard H. Lozier, and Roberto A. Bogomolni, Biochimica et Biophysica Acta **505**, 215 (1979).

8. Daniel J. Müller, Frank A. Schabert, Georg Büldt, and Andreas Engel, Biophys. J. **68**, 1681 (1995).

9. Hans-Jürgen Butt, Eur. Biophys. J. **19**, 31 (1990).

10. Zhongping Chen and Robert F. Birge, Trends Biotech. **11**, 292 (1993).

11. Jin-An He, Lynne Samuelson, Lian Li, Jayant Kumar, and Sukant K. Tripathy, Adv. Mater. **11**, 435 (1999).

12. At least the following exist: CSFM, NCSFM, CPSFM, LFM, EFM, KFM, TMSFM, MFM, NCSTM.

13. Tilman E. Schäffer and Paul K. Hansma, J. App. Phys. **84**, 4661 (1998).

14. D.M. Schaefer, A. Patil, R.P. Andres, and R. Reifenberger, Appl. Phys. Lett. **66**, 1012 (1995).

15. Susanne Kopta and Miquel Salmeron, J. Chem. Phys. **113**, 8249 (2000).

16. Nanosensors Dr. Olaf Wolter GmbH, *Nanosensors*, Nanosensors Dr. Olaf Wolter GmbH, 1999.

17. J.N. Israelachvili, *Intermolecular and Surface Forces, 2nd ed.*, Academic Press, San Diego, 1992.

18. www.spmtips.com.

19. M. Enachescu, D. Schleef, D. F. Ogletree, and M. Salmeron, Phys. Rev. B **60**, 16913 (1999).

20. M. Salmeron, G. Neubauer, A. Folch, M. Tomitori, D. F. Ogletree, and P. Sautet, Langmuir **9**, 3600 (1993).

21. Supriyo Datta, Weidong Tian, Seunghun Hong, R. Reifenberger, Jason I. Henderson, and Clifford P. Kubiak, Phys. Rev. Lett. **79**, 2530 (1997).

22. Yongqiang Xue, Supriyo Datta, Seunghun Hong, R. Reifenberger, Jason I. Henderson, and Clifford P. Kubiak, Phys. Rev. B **59**, R7852 (1999).

23. W. Tian, S. Datta, S. Hong, R. Reifenberger, J.I. Henderson, and C.P. Kubiak, J. Chem. Phys. **109**, 2874 (1998).

24. U. Dürig, O. Züger, and A. Stalder, J. Appl. Phys. **72**, 1778 (1992).

25. Jarry B. Marrion and Stephen T. Thornton, *Classical Dynamics*, Saunders College Publishing, 1995.

26. B. Walsh, MS thesis, 2000, Purdue University (unpublished).

27. Steve Howell, unpublished.

28. Ursula Lehnert, Valerie Réat, Martin Weik, Giuseppe Zaccaï, and Claude Pfister, Biophys. J. **75**, 1945 (1998).

29. I. Hamdy, A. Mostafa, G. Váró, R. Tóth-Boconádi, A. Dér, and L. Keszthelyi, Biophys. J. **70**, 468 (1996).

30. Hans-Jürgen Butt, Kenneth Downing, and Paul K. Hansma, Biophys. J. **58**, 1473 (1990).

31. F. Oesterhelt, D. Oesterhelt, M. Pfeiffer, A. Engel, H. E. Gaub, and D. J. Müller, Science **288**, 143 (2000).

32. Jin-An He, Lynne Samuelson, Lian Li, Jayant Kumar, and Sukant K. Tripathy, J. Phys. Chem. B **102**, 7067 (1998).

33. Jin-An He, Lynne Samuelson, Lian Li, Jayant Kumar, and Sukant K. Tripathy, Langmuir **14**, 1674 (1998).

34. Robert A. Brizzolara, Jennifer L. Boyd, and Ann E. Tate, J. Vac. Sci. Technol. A **15**, 773 (1997).

35. Clemens Möller, Mike Allen, Virgil Elings, Andreas ENgel, and Daniel J. Müller, Biophys. J. **77**, 1150 (1999).

36. Daniel J. Müller and Andreas Engel, Biophys. J. **73**, 1633 (1997).

37. D. L. Worcester, H. S. Kim, R. G. Miller, and P. J. Bryant, J. Vac. Sci. Technol. A **8**, 403 (1990).

38. J. K. Heinrich Hörber, Johannes Mosbacher, Walter Häberle, J. Peter Ruppersberg, and Bert Sakmann, Biophys. J. **68**, 1687 (1995).

39. William F. Heinz and Jan H. Hoh, Biophys. J. **76**, 528 (1999).

40. D. Erts, H. Olin, L. Ryen, E. Olsson, and A. Thölén, Phys. Rev. B **61**, 12725 (2000).

41. B. Ludolph, M. H. Devoret, D. Esteve, C. Urbina, and J. M. van Ruitenbeek, Phys. Rev. Lett. **82**, 1530 (1999).

42. B. Ludolph and J. M. van Ruitenbeek, Phys. Rev. B **59**, 12290 (1999).

43. Gregor Cevc, Biochimica et Biophysica Acta **1031—3**, 331 (1990).

44. E. Barrena, C. Ocal, and M. Salmeron, J. Chem. Phys. **111**, 9797 (1999).

45. E. Barrena, C. Ocal, and M. Salmeron, J. Chem. Phys. **113**, 2413 (2000).